Submitted to Physical Re

LBL-36
Preprint

c.2

INVESTIGATION OF LOW-MASS $K\pi\pi$ SYSTEMS IN 12 GeV/c K^+p INTERACTIONS

Philip J. Davis*, Margaret Alston-Garnjost, Angela Barbaro-Galtieri, Stanley M. Flatté, Jerome H. Friedman, Gerald R. Lynch, Monroe S. Rabin and Frank T. Solmitz

October 1971

AEC Contract No. W-7405-eng-48

*Also filed as a Ph. D. Thesis

DISCLAIMER

INVESTIGATION OF LOW-MASS $K\pi\pi$ SYSTEMS IN 12 GeV/c K^+p INTERACTIONS

Philip J. Davis, Margaret Alston-Garnjost, Angela Barbaro-Galtieri, Stanley M. Flatté, Jerome H. Friedman, Gerald R. Lynch, Monroe S. Rabin and Frank T. Solmitz

Lawrence Berkeley Laboratory
University of California
Berkeley, California 94720

ABSTRACT

We have studied the broad $K\pi\pi$ mass enhancements at 1300 MeV in the reactions 12 GeV/c $K^+p \to pK^+\pi^-\pi^+$ and $pK^0\pi^0\pi^+$. Our data were obtained from a 600 000 picture exposure of the SLAC 82-inch HBC (which corresponds to a path length of 35 events/μb). We observe a two peak substructure in the $K^0\pi^0\pi^+$ mass spectrum at 1260 MeV and 1420 MeV. Our estimated contribution of the $K_N(1420)$ accounts for only about half of the 1420-MeV peak (a discrepancy of about 2.4 standard deviations). The $K^+\pi^-\pi^+$ mass spectrum has a different shape. Further, assuming the $K\pi\pi$ system to be S-wave 1^+ $K_V(890)\pi$ and $\rho(765)K$, we have fitted separately the $K^+\pi^-\pi^+$ and the $K^0\pi^0\pi^+$ Dalitz plots. We obtain inconsistent fits. This inconsistency and the differences in the $K\pi\pi$ mass spectra could be explained by an additional contribution of an I = 0 S-wave $\pi\pi$ state in $K^+\pi^-\pi^+$. The $K\pi\pi$ angular-decay distributions imply the dominance of the spin-parity state 1^+ with $M_z = 0$ along the incident beam direction. However, there are other J^P states and states with $M_z \neq 0$. The 1260-MeV $K\pi\pi$ mass region is produced more peripherally than the 1420-MeV region.

I. INTRODUCTION

A. Purpose and Scope

The $K\pi\pi$ 1.3-GeV mass region, the Q, has been extensively studied.[1-29] (See Ref. 1 for a compilation.) Despite this effort, questions of the existence and/or nature of Q substructure remain unsettled. Interest in Q substructure is due in part to the possible assignments of two resonances to SU(3) nonets with $J^{PC} = 1^{+\pm}$. In the hope of obtaining additional results regarding Q substructure, we analyze the 12-GeV/c K^+p reactions:

(1)	$K^+ p \rightarrow pK^+\pi^-\pi^+$	30 163 events
(2)	$K^+p \rightarrow pK^0\pi^0\pi^+$, $K^0 \rightarrow \pi^-\pi^+$	6431 events
(3)	$K^+p \rightarrow nK^0\pi^+\pi^+$, $K^0 \rightarrow \pi^-\pi^+$	1279 events
(4)	$K^+p \rightarrow pK^0\pi^+$, $K^0 \rightarrow \pi^-\pi^+$	1900 events

The data are from 600 000 pictures of the SLAC 82-inch HBC exposed to an rf-separated 12-GeV/c K^+ beam.[30] For reactions (1) and (2) we select events with a $M(K\pi\pi) < 1.5$ GeV. Reaction (3) is analyzed to corroborate the Q I-spin assignment of 1/2. Reaction (4) is used to determine the $K_N(1420)$ contributions to reactions (1) and (2).

We conclude our introduction with a brief synopsis of the existing Q data and a summary of our results. In section II we discuss the data reduction and emphasize the problem of $K^+\pi^+$ ambiguity in reaction (1). Section III deals first with the $K\pi\pi$ mass spectra, secondly with the failure of the $K_N(1420)$ to account fully for our observed $K^0\pi^0\pi^+$ mass structure, and thirdly with detailed studies, including Dalitz-plot fits. In Section IV we summarize our results and compare them with three similar experiments.

B. Brief Synopsis of Existing Q data

The existing Q data are derived from two basic sets of experiments: first, those which observe a diffractive $K\pi\pi$ enhancement in a reaction of the kind $K\,T \rightarrow K\pi\pi T$, where T is some target; and secondly, those which observe a $K\pi\pi$ enhancement in nondiffractive reactions. The first experiments agree generally that: (1) the Q is a broad $K\pi\pi$ enhancement peripherally produced, (2) the Q decays predominately into $K_V(890)\pi$ but also into $\rho(765)K$, (3) the Q has I-spin 1/2, and (4) the Q has spin parity 1^+ favored, but with 2^- still possible. These same experiments differ in their conclusions regarding Q structure. Several report two or more resonances in the Q region.[7,8,29] Some report structure with a 1420-MeV peak accounted for by the $K_N(1420)$.[17,27] In contrast, other experiments report that the $K_N(1420)$ fails to account fully for their observed 1420-MeV peak.[14,25] In contrast to a resonant interpretation, several experiments obtain reasonable fits to their data by Deck or double-Regge-pole models, e.g., diffractive dissociation of the beam into $K_V(890)\pi$ with the π then elastically scattering off the target.[12,15,20,22] (Usually the $K_V(890)\pi$ mass spectrum is the least well fitted kinematic variable.) Because of duality, the resonant and Deck descriptions may be theoretically compatible.[31] At the 1970 Philadelphia Conference, Firestone reviewed the $K^{\pm}p$ experiments from 2.15 to 13 GeV/c.[28] By fitting the $K\pi\pi$ mass distributions, he concluded that a simple Breit-Wigner shape does not fit the Q peak, but that two Breit-Wigner shapes do give reasonable fits at all energies.

Besides the above diffractive experiments, there are some nondiffractive experiments with either a $\bar{p}$ or π^- beam.[2-5]

Most significant among these is that of Astier et al. who find evidence in $\bar{p}p \to \bar{K}K\pi\pi$ for a $K\pi\pi$ resonance, the C-meson, with a mass and width of 1242^{+9}_{-10} MeV and 127^{+7}_{-25} MeV.[4] The C-meson branching ratios into $K_V(890)\pi$ and $\rho(765)K$ are (0.25 ± 0.1) and (0.75 ± 0.1). They assign to the C-meson the quantum numbers $J^{PC} = 1^{++}$. Crennell et al. find evidence for production of two $K\pi\pi$ enhancements in 6-GeV/c $\pi^- p \to \Lambda K\pi\pi$: one at about 1440 MeV, which they associate with the $K_N(1420)$; and the other at about 1300 MeV.[3] They favor a resonant interpretation for the 1300-MeV enhancement and assign it a narrow width of about 60 MeV, an I-spin of 1/2, and decay modes into both $K_V(890)$ and $\rho(765)K$.

In summary, the diffractive experiments have generally broad $K\pi\pi$ enhancements, either with or without substructure. The relatively narrow enhancements seen by Astier et al. and Crennell et al. complicate the interpretation of the diffractive Q data.

C. Results

We find evidence for a two-peak $K^0\pi^0\pi^+$ mass spectrum (see Fig. 1). The low-Q peak, which we shall label Q_L, is centered at about 1260 MeV with a full-width of about 120 MeV, and the high-Q peak, which we shall lable Q_H, is centered at about 1420 MeV with a full-width of about 80 MeV. These values are quite dependent upon the assumed background. Using the known $K_N(1420)$ branching ratios and the amount of $K_N(1420) \to K^0\pi^+$ determined for reaction (4), we calculate the $K_N(1420)$ contributions to the $K\pi\pi$ mass spectra (see the shaded areas of Fig. 1). The $K_N(1420)$ accounts only for about half of the observed $K^0\pi^0\pi^+$ peak at 1420 MeV. The $K^+\pi^-\pi^+$ spectrum has a shape different from that of $K^0\pi^0\pi^+$. The differences in the $K\pi\pi$ mass spectra may be explained by a contribution to the Q of

$\epsilon(700)K$, $\epsilon(700) \to \pi^-\pi^+$, where by $\epsilon(700)$ we mean only an I-spin zero S-wave $\pi\pi$ state and not necessarily a resonance. The $\epsilon(700)K$ can contribute to $K^+\pi^-\pi^+$, but not to $K^0\pi^0\pi^+$. The ratio of the number of $K^0\pi^0\pi^+$ to $K^+\pi^-\pi^+$ events gives added support for an $\epsilon(700)K$ mode. For pure $\epsilon(700)K$, $\rho(765)K$, and $K_V(890)\pi$ this ratio would be 0, 2, and 1, respectively. Despite the presence of significant $\rho(765)K$ in our data, the ratio is unity within errors (6%) for four Q mass subdivisions. This result is similar to that obtained by Alexander et al. who originally suggested the possible contribution of the $\epsilon(700)K$.[14]

Our Q decay-plane-normal distributions and the $Q \to K(890)\pi$, $K_V(890) \to K^+\pi^-$ two-body angular-decay distributions imply that $J^P = 1^+$ is favored. However, we can exclude neither $J^P = 0^-$ nor 2^-. With the assumption that the Q is in a $J^P = 1^+$ state, an analysis of the $Q \to K_V(890)\pi$, $K_V(890) \to K^+\pi^-$ two-body angular-decay distributions indicates that the $Q \to K_V(890)\pi$ decay is predominantly S-wave with zero spin projection along the beam, $M_z = 0$. However, the Q has significant non S-wave 1^+ components and significant components with $M_z \neq 0$.

We determine the Q decay modes by fitting separately the $K^+\pi^-\pi^+$ and $K^0\pi^0\pi^+$ Dalitz plots to S-wave 1^+ $K_V(890)\pi$ and $\rho(765)K$ for four $K\pi\pi$ mass subdivisions. We perform both incoherent and partially coherent fits. Interference effects are important. The fraction of $\rho(765)K$ in $K^0\pi^0\pi^+$ ranges between (0.24 ± 0.06) and (0.37 ± 0.05) for different $K\pi\pi$ mass regions. Using the $K^0\pi^0\pi^+$ fitted results and assuming pure S-wave 1^+, we estimate that the $\epsilon(700)K$ contribution in $K^+\pi^-\pi^+$ consists of a fraction ranging from (0.03 ± 0.08) to (0.22 ± 0.06), the lower values applying to low $K\pi\pi$ masses and the higher to the 1420-MeV region.

II. Data Reduction

A. Scanning and Measuring

All pictures were at least twice-scanned and ten percent of the film was thrice-scanned.[32] Reaction (1) corresponds to a four-prong topology. Reactions (2) through (4) correspond to a vee two-prong topology. We use the Derenzo-Hildebrand method to calculate scan efficiencies.[33] (For our experiment this method yields slightly smaller values than the traditional Geiger-Werner method.) The first scan four-prong and vee two-prong efficiencies are 0.97 and 0.90.[34] With exclusion of non-beam events and measurer rejects of invalid events, a total of about 189 000 four-prongs and 38 000 vee two-prongs were measured with the Spiral Reader. The LBL Group A programs -- POOH, TVGP, and SQUAW -- were used in the data reduction . Failing events were measured a second time, and of the twice-failing events, half were measured a third time.[35] The measuring and scanning results are summarized in Table I.

B. Path Length

Three methods are used in calculating the path length.[34] They use, respectively: (1) the number of τ decays, (2) the number and length of beam tracks, and (3) the total number of events normalized to the known total cross section. These three methods give for the path length, respectively: (34.7 ± 0.9), (35.2 ± 0.6), and (34.0 ± 1.2) events/μb. The weighted average is (34.9 ± 0.5) events/μb. (Small correlations are neglected.) The weighted average has a χ^2 of 0.8 for 2 degrees of freedom. Despite this good agreement we use as our final answer (34.9 ± 1.0) events /μb, because of possible systematic errors in our results. Table II is a summary of the cross sections for reactions (1) through (4) calculated using the efficiencies and path length in Table I.

C. Fit Ambiguities

1. Final State $pK^+\pi^-\pi^+$

All successfully measured four-prongs are fitted to the final state hypotheses: (a) $pK^+\pi^-\pi^+$, (b) $pK^+K^-K^+$, and (c) $pK^+\bar{p}p$. The best fit is defined as the fit with the minimum sum of kinematic chi-square, χ^2_K, and bubble-density chi-square, χ^2_{BD}. The bubble-density chi-square is calculated using the pulse-height information of Spiral Reader measurements.[36] In addition, a fit is required to have a χ^2_K corresponding to a confidence level greater than 10^{-5}.

Best fits to $pK^+\pi^-\pi^+$ have a 26% ambiguity including permutations of the track identities. For our study of the Q region we selected events with $M(K\pi\pi) < 1.5$ GeV and $M(p\pi^+) > 1.5$ GeV. The $p\pi^+$ mass cut removes events with a $\Delta^{++}(1236)$ present. With these selections, best fits to $pK^+\pi^-\pi^+$ have a 40% permutation ambiguity, a 3% ambiguity with $pK^+K^-K^+$, and a 4% ambiguity with $pK^+\bar{p}p$ (see Table III). We proceed to discuss each of these ambiguities in detail. Since the Q is produced peripherally, the outgoing proton is easily identified; but interchanging the K^+ and π^+ identifications results only in a slight change of the energy balance when the K^+ and π^+ have nearly the same lab momentum. Likewise, since the K^+ and π^+ are usually both minimum ionizing, there is little difference in the χ^2_{BD} for permutation ambiguities.

To estimate the fraction and effects of having the wrong permutation fit best, we generate two Monte Carlo samples of track measurements and then process them as actual measurements.[37] The first Monte Carlo sample corresponds to a $K^+\pi^-\pi^+$ resonance peripherally produced ($e^{9t}pp$), and with a mass of 1300 MeV, a width of 300 MeV, and an S-wave decay into $K_{V(890)}\pi$.

The $K_V(890)$ decay into $K^+\pi^-$ is given a $\cos^2\theta$ distribution with respect to the beam. As with the data, we require a $M(K\pi\pi) < 1.5$ GeV and a $M(p\pi^+) > 1.5$ GeV. Of 439 generated events, 42% have a permutation ambiguity. Of these ambiguities, (19 ± 3) % have the wrong permutation fitting best. The second Monte Carlo sample corresponds to an analogous $\rho(765)K$ decay of the Q. Of 438 generated events, 47% have a permutation ambiguity of which (15 ± 3) % have the wrong permutation fitting best. Therefore we estimate that 8% of all $K^+\pi^-\pi^+$ events in the Q region are ambiguous with the wrong permutation fitting best. In addition, we find for the two Monte Carlo samples, respectively, that (1.6 ±0.6)% and (0.7 ±0.4)%of generated Q events have a wrong permutation fit passing and the correct permutation fit failing. Thus, we estimate that about 10% of all real $K^+\pi^-\pi^+$ events in the Q region correspond to the wrong $K^+\pi^+$ permutation.

The $K^+\pi^+$ misidentification produces a serious bias in our $K^+\pi^-\pi^+$ data for the Q. The above Monte Carlo samples indicate that actual $K_V(890)\pi$ events with $K^+\pi^+$ misidentification result in a $\pi^-\pi^+$ mass peaking at about 720 MeV, and in a fairly uniform $K^+\pi^-$ mass spectrum. Wrongly identified $\rho(765)K$ events result in $K^+\pi^-$ mass spectrum spread out between 780 and 1000 MeV, and in a $\pi^-\pi^+$ mass spectrum spread out between 440 and 810 MeV. For the $K_V(890)\pi$ misidentification, the $K\pi\pi$ mass has an average shift of +10 MeV with a spread of ±20 MeV.

Best fits to $pK^+\pi^-\pi^+$ ambiguous with $pK^+K^-K^+$ or $pK^+\bar{p}p$ comprise 7% of all $K^+\pi^-\pi^+$ events in the Q region. After examining a sample of these ambiguities on the scan table, we decided that by a selection upon the bubble-density chi-square, we could reduce the contamination of $pK^+K^-K^+$ and $pK^+\bar{p}p$ to 1% and 2%, respectively, (See Table III).

2. Final States $pK^0\pi^0\pi^+$ and $nK^0\pi^+\pi^+$

Both final states $pK^0\pi^0\pi^+$ and $nK^0\pi^+\pi^+$ correspond to a vee two-prong topology with a 1-C fit at the production vertex and a 3-C fit at the vee vertex for the K^0 decay into $\pi^-\pi^+$. A special study of ambiguities led to the following selection criteria for production 1-C fits: (1) no production 4-C fit with a confidence level (C. L.) greater than 10^{-5}, (2) a production 1-C fit with a kinematic C. L. $> 10^{-3}$, and (3) a bubble-density chi-square, χ^2_{BD}, less than five plus the minimum bubble-density χ^2 of all fits. The best fit is chosen as the one which has the minimum sum of kinematic and bubble-density χ^2s. There are no serious ambiguities for the final state $pK^0\pi^0\pi^+$. With no cuts, 15% of all events with a best fit to $pK^0\pi^0\pi^+$ are ambiguous. With selection on a $M(K\pi\pi) < 1.5$ GeV, 9% are ambiguous. These events have a 3% ambiguity with the final state $pK^0K^+(\bar{K}^0)$ where one of the two K^0's is undetected, and a 5% ambiguity with $n\bar{K}^0K^+K^+$ (see Table III). In addition to 1-C fit ambiguities, there is the possibility of single π^0 events being faked, for example, by poorly measured $2\pi^0$ events. To estimate this type of background, we calculate the missing-mass square for all non 4-C events assuming $K^+p \rightarrow pK^0\pi^+(MM)$. With a further restriction to events for which the proton momentum in the lab is less than 1 GeV/c, the resulting mass-square distribution is plotted in Fig. 2(a), wherein the shaded area corresponds to events which have a best fit to the final state $pK^0\pi^0\pi^+$. For a linear background under the π^0 peak, the background is less than 4% of the π^0 signal for events in the π^0 region.

The final state $nK^0\pi^+\pi^+$ has a 44% ambiguity before selection on Q events. With selection on a $M(K\pi\pi) < 1.5$ GeV, the total $nK^0\pi^+\pi^+$ ambiguity is 16%. The missing-mass square for the

hypothesis $K^+p \to K^0\pi^+\pi^+$(MM) is plotted in Fig. 2(b) for non-4 C events with both a MM system momentum in the lab less than 1 GeV/c and a $M(K^0\pi^+\pi^+)$ less than 1.5 GeV. The shaded area corresponds to events with a best fit to $nK^0\pi^+\pi^+$. We have not studied these ambiguities further since we only use the number of events to obtain an upper limit for the Q branching ratio into $K^0\pi^+\pi^+$.

III. Data Analysis

In this section we discuss (A) the $K\pi\pi$ mass spectra, (B) the $K_N(1420)$ contribution to the $K\pi\pi$ mass spectra, (C) the recoil-proton momentum-transfer, (D) the decay-plane-normal distribution, (E) the Q and $K_V(890)$ two-body angular-decay distributions, and (F) the $K\pi\pi$ Dalitz plots, including our fits to them.

A. $K\pi\pi$ Mass Distributions

The major evidence we have for Q substructure is the $K\pi\pi$ mass distributions given in Figs. 1 and 3. Figure 1 corresponds to no cuts. (The shaded areas are the estimated $K_N(1420)$ contributions discussed below.) Figures 3(a) and 3(b) correspond to three cuts: $M(K\pi\pi) < 1.5$ GeV, $M(p\pi^+) > 1.5$ GeV, and in addition $-t_{pp} < 1$ GeV^2. In all subsequent reference to Q events or Q selection these three cuts are implicit unless otherwise specified. The shaded areas of Fig. 3 and of subsequent $K^+\pi^-\pi^+$ plots correspond to best fits which have a permutation ambiguity. The $p\pi^+$ mass cut removes events with a $\Delta^{++}(1236)$ present. By examining the baryon angular-decay distributions, we estimate that the final states $pK^+\pi^-\pi^+$ and $pK^0\pi^0\pi^+$ each have less than 2.5% of resonant $p\pi^+$ remaining. The $K^0\pi^0\pi^+$ mass spectra have a two-peak substructure -- which we label Q_L and Q_H. Any mass and width values assigned to the Q_L and the Q_H are very background-dependent. The Q_L peaks at a mass of about 1260 MeV

with a width of about 120 MeV, and the Q_H peaks at a mass of about 1420 MeV with a width of roughly 80 MeV.

The $K^+\pi^-\pi^+$ mass spectrum has a different shape from the $K^0\pi^0\pi^+$ spectrum. The effect of $K^+\pi^+$ misidentification, which washes out structure to some extent, is not large enough to explain this difference. Also, the differences in resolutions cannot account for the different shapes of the two spectra (see Table IV). However, this difference may be explained by an $\epsilon(700)K$ contribution -- which is allowed for $K^+\pi^-\pi^+$, but not for $K^0\pi^0\pi^+$. By $\epsilon(700)$ we mean an I = 0 S-wave $\pi\pi$ state and not necessarily a resonant state. One way an $\epsilon(700)K$ contribution could "fill in" the 1.36-GeV mass region is an $\epsilon(700)K$ Deck-like contribution (which peaks in this region).

We attempt to enhance substructure in the $K\pi\pi$ mass spectra by selecting on a vector meson or on t_{pp} regions. Selection on a $K_V(890)$ or $\rho(765)$ being present yields the $K\pi\pi$ mass spectra given in Figs. 3(c) and (d).[41] Figures 3(e) and (f) correspond to $K_V(890)$ selection. (The shaded areas correspond to events with a permutation ambiguity.) Both selections reduce the significance in the $K^0\pi^0\pi^+$ mass spectrum of the dip at 1360 MeV and reduce the 1420 MeV mass region to a flat shoulder. Thus, neither selection enhances Q substructure.

Selection on different t_{pp} regions enhances different regions of $K\pi\pi$ mass. Selecting on either $-t_{pp} < 0.1$ GeV^2, $0.1 < -t_{pp} < 0.3$ GeV^2, or $-t_{pp} > 0.3$ GeV^2, we obtain the $K\pi\pi$ mass distributions given in Fig. 4. Since the minimum $-t_{pp}$ is less than 0.006 GeV^2, our use of t_{pp} is practically equivalent to $t'_{pp} = t_{pp} - \min t_{pp}$. Events in the 1260-MeV region are produced more peripherally than in the 1420-MeV region.

In addition we have examined the final state $nK^0\pi^+\pi^+$ for a Q enhancement. The Q decay mode into $\rho(765)K$ is forbidden for this final state since $\pi^+\pi^+$ is a pure I = 2 state. In Figure 5 we plot the $K^0\pi^+\pi^+$ mass for events with $-t_{pn} < 1$ GeV^2. Assuming all $K^0\pi^+\pi^+$ events in the Q region (126 events) to be pure $K_V(890)\pi$, we estimate that the I = 3/2 $K_V(890)\pi$ contribution to the Q is less than about 2% of the I = 1/2 contribution wherein we have corrected for the production and decay Clesbch-Gordan I-spin coefficients. We therefore agree with the accepted I-spin Q assignment of 1/2.

B. Contribution of the $K_N(1420)$

The $K_N(1420)$ three-body decay modes contribute to the high side of the Q mass spectra. We determine its contributions by studying the reaction $K^+p \to pK^0\pi^+$. The amounts of $K_N(1420) \to K\pi\pi$ are estimated by a two-step procedure. First, the amount of $K_N(1420) \to K^0\pi^+$ in the final state $pK^0\pi^+$ is determined by a maximum likelihood fit to the $K^0\pi^+$ mass spectrum. Second, the $K_N(1420)$ branching ratios are used to calculate the amounts in $K\pi\pi$.

1. Two-Body $K_N(1420)$

Before discussing the two-body fits, we note that there are no serious biases in the production 4-C fits to the final state $pK^0\pi^+$ for events with a $K\pi$ mass near 1420 MeV. We fit the $K^0\pi^+$ mass distribution to a D-wave Breit-Wigner and a linear background (see Fig. 6). The differential rate is given by:

$$\frac{dN}{dm} = N \times B \times \left[1 + BW \frac{(p_R/m_R)}{(p/m)}\right], \qquad (1)$$

where N is a total normalization constant; B is a linear background given by

$$B = 1 + s \frac{m-\bar{m}}{m_H - m_L}, \qquad (2)$$

wherein $\bar{m} = (m_L + m_H)/2$ and s is the slope of the background. The lower and upper mass bounds are m_L and m_H. The D-wave Breit-Wigner is given by

$$BW = \frac{r}{1-r} \frac{(\Gamma_R/2)\,[\Gamma(m)/2]}{(m-m_R)^2 + [\Gamma(m)/2]^2}, \qquad (3)$$

where r is the ratio of signal to signal-plus-background, m is the $K\pi$ mass, p is the K momentum in the $K\pi$ center-of-mass, $\Gamma(m)$ is the mass-dependent width of the resonance, and m_R, p_R, Γ_R are the corresponding resonant values. The form used for $\Gamma(m)$ is

$$\Gamma(m) = \Gamma_R \frac{[p^2/(p^2 + X^2)]^2 (p/m)}{[p_R^2/(p_R^2 + X^2)]^2 (p_R/m_R)} \qquad (4)$$

where X equals 100 MeV.[42] We perform a maximum likelihood fit of m_R, Γ_R, s, and r to the $K^0\pi^+$ mass spectrum from 1200 to 1650 MeV and summarize the results in Table V. The fitted mass distribution is given in Fig. 6. The fitted number of $K_N(1420)$ is $(243 \pm {}^{42}_{38})$ events. Our value of m_R, (1420 ± 10) MeV, agrees with the Particle Data Group's compilation value of (1408 ± 4) MeV.[1] Our value for Γ_R, $(136 \pm {}^{42}_{30})$ MeV, agrees (within errors) with the Particle Data Group's value of (107 ± 15) MeV. If in the above fit we restrict m_R and Γ_R to the compiled values, we obtain (208 ± 30) events for the fitted amount of $K_N(1420) \to K^0\pi^+$ instead of $(243 \pm {}^{42}_{38})$ events. Since the error for the latter amount includes the uncertainty in the values of m_R and Γ_R, we use it in the calculations for the amount of three-body $K_N(1420)$. Corrected for vee detection inefficiency the number of events is (289 ± 46).

2. Three-Body $K_N(1420)$

The $K_N(1420)$ contributions to $K\pi\pi$ with no $p\pi^+$ mass selection can be estimated by using the above two-body amount and the $K_N(1420)$

branching ratios given by other experiments. For the $K_N(1420)$ branching ratios we use the fitted values given by the Particle Data Group: $K\pi/\text{Total} = (0.569 \pm 0.040)$, $K_V(890)\pi/\text{Total} = (0.27 \pm 0.032)$, and $\rho(765)K/\text{Total} = (0.092 \pm 0.035)$.[1] The $K_N(1420)$ branching ratios and the observed amount of $K_N(1420) \rightarrow K^0\pi^+$ yield a prediction of (140 ± 32) events for $K_N(1420) \rightarrow K^0\pi^0\pi^+$. With additional factors for the unobserved K^0 decays and the measurement efficiencies of the vee two-prongs and the four-prongs, the predicted amount of $K_N(1420) \rightarrow K^+\pi^-\pi^+$ is (359 ± 77) events. These predictions are indicated by the shaded areas in the uncut $K\pi\pi$ mass plots of Fig. 1. Assuming a linear background under the 1420-MeV peak as indicated in the $K^0\pi^0\pi^+$ mass plot, we estimate (135 ± 15) events above background in the mass range 1.36 to 1.48 GeV. In this mass range, the estimated amount of $K_N(1420)$ is (78 ± 18) so that the prediction is about 2.4 standard deviations too small.

C. t_{pp} Distributions

The t_{pp} distributions are given in Fig. 7 for Q events in $pK^+\pi^-\pi^+$ and $pK^0\pi^0\pi^+$. Since the minimum t_{pp} is less than 0.006 GeV^2, t_{pp} is practically equivalent to t_{pp} - min t_{pp}. In Fig. 8 are plotted the corresponding t_{pp} spectra for our four $K\pi\pi$ mass regions -- 1.1 to 1.2 GeV, 1.2 to 1.27 GeV, 1.27 to 1.36 GeV, and 1.36 to 1.46 GeV.[43] (Note in Fig. 8 that the $pK^+\pi^-\pi^+$ events are plotted with a bin size of 0.05 GeV^2 and the $pK^0\pi^0\pi^+$ events with one of 0.1 GeV^2.) The spectra have a change of slope at $t_{pp} \approx -0.5$ GeV^2. Therefore we perform minimum chi-square fits of $Ae^{Bt_{pp}}$ to each of these spectra over the restricted range in $|t_{pp}|$ of 0.0 to 0.4 GeV^2. The results of these fits are summarized in Table VI. The fits to $pK^+\pi^-\pi^+$ are generally poor due to large chi-square contributions from the first and/or

second bins. As is evident from the t_{pp} distribution of $K^+\pi^-\pi^+$ for the entire Q region (see Fig. 7), a parametrization of $Ae^{Bt_{pp}}$ is inadequate and gives a very small confidence level for the fit. The $pK^0\pi^0\pi^+$ fits with poorer statistics are better, but still poor. The value of B decreases from about 9 to 6 GeV^{-2} over our four $K\pi\pi$ mass intervals. The $K^+\pi^-\pi^+$ events appear to be somewhat more peripherally produced than the $K^0\pi^0\pi^+$ events.

To estimate the contribution of the $K_N(1420)$ to the t_{pp} spectra of $K\pi\pi$ in region IV, 1.36 to 1.46 GeV, we fit $Ae^{Bt_{pp}}$ to the t_{pp} spectrum of the reaction $K^+p \rightarrow pK^0\pi^+$. To test for the possibility that the background under the $K_N(1420)$ has a different t_{pp} distribution, we perform three minimum chi-square fits to the $K^0\pi^+$ mass intervals -- (i) 1.20 to 1.35 GeV, (ii) 1.35 to 1.50 GeV, and (iii) 1.50 to 1.65 GeV. The results of these fits are summarized in Table V and the t_{pp} spectra are plotted in Fig. 9. Intervals (ii) and (iii) are in good agreement. The somewhat larger B value for interval (i) might correspond to the tail of the $K_V(890)$. Thus, we find that the background has approximately the same t_{pp} distribution as the $K_N(1420)$ which has a B value of (2.3 ± 0.8) GeV^{-2}.

The $K_N(1420)$ contributions to the t_{pp} spectra in $pK^+\pi^-\pi^+$ and $pK^0\pi^0\pi^+$ are calculated by scaling the t_{pp} spectrum of the $K\pi$ mass interval (ii) in a manner analogous to that used to estimate the $K\pi\pi$ mass contribution in section III. B. 2. These estimates for $K\pi\pi$ mass region IV are plotted in Fig. 10. Though the statistics are quite poor, these estimates account for only about half of the events with $-t_{pp} > 0.5$ GeV^2. Clearly the contribution of the $K_N(1420)$ does not change appreciably the slopes given in Table VI.

D. Q Decay-Plane-Normal

If the Q were entirely diffractively produced, the Q would have unnatural spin-parity and zero spin-projection along the incident K. We define axes in the Q rest frame -- the beam direction as the z-axis and the production-plane-normal as the y-axis. For $M_z = 0$ the unnatural spin-parities 0^-, 1^+, and 2^- have Q decay-plane-normal distributions of uniform, $\sin^2\Theta$, and

$$\left(\frac{9}{4} + A\right)\sin^4\Theta - 3\sin^2\Theta + 1$$

where Θ is the angle between the normal and the beam direction and A is a positive number.[25] Unnatural spin-parity states can decay into $K\pi\pi$, but not into $K\pi$; whereas natural spin-parity states can decay into both. The absence of a Q peak in the $K^0\pi^+$ mass distribution of the reaction $K^+p \to pK^0\pi^+$ (see Fig. 6) makes it plausible that the Q consists predominantly of unnatural spin-parity states except for the $K_N(1420)$ contribution of 2^+ to the high side of the Q.

For our four $K\pi\pi$ mass regions -- 1.1 to 1.2 GeV, 1.2 to 1.27 GeV, 1.27 to 1.36 GeV, and 1.36 to 1.46 GeV -- we plot the Q decay-plane-normal cos Θ and Φ distributions in Figs. 11 and 12. (The shaded areas of the $K^+\pi^-\pi^+$ plots correspond to events with a permutation ambiguity.) We find the cos Θ distributions are predominately $\sin^2\Theta$ so that the Q is predominantly 1^+ with $M_z = 0$. However, the nonvanishing of the distributions near $\cos\Theta = \pm 1$ necessitates the presence of other spin states. Admixtures of 0^-, 1^+, and 2^- with the variable A adjusted can fit the cos Θ distributions. There is neither any striking variation in the shapes of the distributions for different $K\pi\pi$ mass regions nor any major disagreement between $K^+\pi^-\pi^+$ and $K^0\pi^0\pi^+$. All the Φ distributions are consistent with being

uniform as one would expect for $M_z = 0$.

The $p\pi^+$ mass cut, $M(p\pi^+) > 1.5$ GeV, suppresses events with $\cos\Theta \sim 0$; and the effects of this cut are different for $K^0\pi^0\pi^+$ and $K^+\pi^-\pi^+$ since the π^+ distribution in $K^0\pi^0\pi^+$ is different from that in $K^+\pi^-\pi^+$ due to the presence of two $K_V(890)$'s instead of one. Despite these difficulties, we bravely calculate average values of the spherical harmonics up through Y_{66}. In Table VII we list those moments which are non-zero by at least two standard deviations for several $K\pi\pi$ mass regions. The moment $\langle Y_{20} \rangle$ is the most significant. Furthermore, the $K^0\pi^0\pi^+$ values are systematically smaller in absolute value than the $K^+\pi^-\pi^+$ values. This effect indicates possibly different production processes for $K^0\pi^0\pi^+$ and $K^+\pi^-\pi^+$. In addition, spin states with $M_z \neq 0$ are implied by the systematically negative values of $\langle \mathrm{Re}\, Y_{21} \rangle$. (A Monte Carlo calculation demonstrates that this effect is not merely due to the $p\pi^+$ mass cut.) The L = 4 moments, which correspond in part to $J^P = 2^-$ and/or 2^+, are consistent with zero except for a slight deviation from zero of the $K^+\pi^-\pi^+$ values of $\langle \mathrm{Re}\, Y_{43} \rangle$. In summary, the Q decay-plane-normal distributions imply the dominance of $J^P = 1^+$ with $M_z = 0$; but in addition there are other J^P states as well as states with $M_z \neq 0$.

E. Q and $K_V(890)$ Two-Body Angular-Decays

In our analysis of the $Q \to K_V(890)\pi$ and $K_V(890) \to K\pi$ angular decay distributions we consider only the final state $pK^+\pi^-\pi^+$ for which there is just one $K_V(890)$ possible. For a Q with $J^P = 1^+$, the decay into $K_V(890)\pi$ is either S-wave or D-wave. The S-wave decay

corresponds to a uniform decay of the Q into $K_V(890)\pi$. For a Q with $J^P = 1^+$ and $M_z = 0$, the S-wave decay into $K_V(890)\pi$ leads to a $\cos^2\theta_{K_V}$ decay-distribution of the $K_V(890)$ into $K\pi$. We take the $K_V(890)$ and K^+ as decay indicators and define the z- and y-axes as along the beam and production-plane-normal in the Q rest frame. With an additional mass selection on $K_V(890)$, the $\cos\theta_Q$ and Φ_Q distributions are given in Fig. 13 for our four $K\pi\pi$ mass regions -- 1.1 to 1.2 GeV, 1.2 to 1.27 GeV, 1.27 to 1.36 GeV, and 1.36 to 1.46 GeV. The $\cos\theta_Q$ distributions have a backward peak. Two effects complicate the interpretation of this behavior. First, the $p\pi^+$ mass cut suppresses events with $\cos\theta_Q \sim 1$. This effect becomes broader and more pronounced for larger $K\pi\pi$ mass. Second, and more important, the observed backward peaking in $\cos\theta_Q$ is mostly due to background, which is more pronounced for larger $K\pi\pi$ mass. The background includes $K^+\pi^+$ misidentification, $\rho(765)K$, and possibly $\epsilon(700)K$. In addition for region IV about 80 events of $K_N(1420)$ contribute to the backward peak in $\cos\theta_Q$. These $K_N(1420)$ events have an approximately $(Y_{20})^2$ distribution in $\cos\theta_Q$. These effects account largely for the variation in the $\cos\theta_Q$ distributions from regions I to IV. Because of these effects and the large number of the possible contributions of the spin-parity states -- 0^-, S-wave 1^+ with either $M_z = 0$ or $M_z = \pm 1$, D-wave 1^+, 2^-, and 2^+ -- we do not attempt any fits.

If the Q spin states all had $M_z = 0$, then the Φ_Q distributions would be uniform. The non-flatness of the Φ_Q distributions in Fig. 13 constitutes further support for the presence of Q spin states with $M_z \neq 0$.

The corresponding $K_V(890)$ decay distributions are given in Fig. 14. The axes are the same as before and the K^+ is taken as the decay indicator. The large positive asymmetries in the $\cos\theta_{K_V}$ distributions can be explained in terms of $K_V(890)\pi$ interfering with $\rho(765)K$. The ϕ distributions are consistent with being flat.

F. $K\pi\pi$ Dalitz Plots

In this section we present first the general features of the $K\pi\pi$ Dalitz plots and then proceed to discuss our fits.

1. General Features

The $K\pi\pi$ Dalitz plots are given in Fig. 15. For $K^+\pi^-\pi^+$ there is only one $K\pi$ combination for $K_V(890)$, while for $K^0\pi^0\pi^+$ there are two. The curves correspond to the Dalitz plot boundary for a $K\pi\pi$ mass of 1.32 GeV. The corresponding two-body mass plots are given in Figs. 16 and 17. (The shaded areas correspond to events with a permutation ambiguity.) The $K_V(890)\pi$ contribution is dominant, but there is also a significant $\rho(765)K$ contribution.

2. Dalitz Plot Fits

We present fits to the $K\pi\pi$ Dalitz plots for each of our four $K\pi\pi$ mass regions -- 1.1 to 1.2 GeV, 1.2 to 1.27 GeV, 1.27 to 1.36 GeV, and 1.36 to 1.46 GeV. First we discuss the objectives, complications, and formalism of the fits. Secondly, we present the $K^0\pi^0\pi^+$ fits, and next the $K^+\pi^-\pi^+$ fits. Thirdly, we compare the fits and estimate the $\epsilon(700)K$ contribution.

(a) Formalism of the fits. The objectives of the Dalitz-plot fits are to determine (1) the $\rho(765)K$ relative to $K_V(890)\pi$ contributions, (2) the consistency between the $K^0\pi^0\pi^+$ and $K^+\pi^-\pi^+$ fits, and (3) the $\epsilon(700)K$ contribution. Complications include the possible presence of D-wave 1^+ in addition to the dominant S-wave 1^+ as well as other spin states -- 0^-, 2^-, and 2^+. The $K^+\pi^-\pi^+$ fits have an additional complication due to $K^+\pi^+$ misidentification. Bearing in

mind these objectives and complications, we chose to approximate the Q as S-wave 1^+ $K_V(890)\pi$ and $\rho(765)K$. The $\rho(765)K/K_V(890)\pi$ branching ratios are then determined by the $K^0\pi^0\pi^+$ fits, for which there is neither $K^+\pi^+$ misidentification nor an $\epsilon(700)K$ contribution. For the $K^+\pi^-\pi^+$ fits a simple correction for $K^+\pi^+$ misidentification is calculated. The corrected $K^+\pi^-\pi^+$ fits are compared with the $K^0\pi^0\pi^+$ fits. The $\epsilon(700)K$ contribution is estimated by using the $K^0\pi^0\pi^+$ fitted results to calculate the expected amount of $K_V(890)\pi$ and $\rho(765)K$ in $K^+\pi^-\pi^+$. Any difference with the actual number of $K^+\pi^-\pi^+$ events is attributed to an $\epsilon(700)K$ contribution.

We use a formalism for an S-wave $1^+K_V(890)\pi$ and $\rho(765)K$ decay of the Q. Expressing the Dalitz plot intensity in terms of a density matrix, d_{ij}, for the $K_V(890)\pi$ and $\rho(765)K$ amplitudes, we perform two classes of fits -- incoherent fits to the diagonal elements and unconstrained fits to the entire density matrix. The Dalitz-plot intensity, I, is fitted to [20]

$$I = \sum_i d_{ii} |G_i|^2 + \sum_{i<j} 2\left[(\text{Re } d_{ij})(\text{Re } G_i^* G_j) - (\text{Im } d_{ij})(\text{Im } G_i^* G_j)\right]\hat{p}_i \cdot \hat{p}_j, \quad (5)$$

where the indices i and j refer to $K_V(890)\pi^+$, $\rho(765)K$, and $K_V(890)\pi^0$, respectively, for values of 1, 2, and 3. The G_i are P-wave Breit-Wigner's for the vector meson decays. We use the form:

$$G = F \frac{\sqrt{\Gamma(p_V/p)(m/m_V)}}{(m^2 - m_V^2) - im_V\Gamma} \quad (6)$$

where

$$\Gamma = \Gamma_V \left(\frac{p}{p_V}\right)^3 \left(\frac{m_V}{m}\right) \quad (7)$$

with m the vector-meson mass, p the vector-meson decay-product momentum, m_V and p_V the corresponding central values, Γ_V the vector- meson width, and F the appropriate product of Clesbsch-Gordan

I-spin coefficients for the Q and vector-meson decays. The $\hat{p}_i$ are the vector-meson decay-product momentum directions with respect to axes fixed in the Q rest frame. The density matrix elements, d_{ij}, are proportional to products of the $K_V(890)\pi$ and/or $\rho(765)K$ couplings. The d_{ij} are normalized so that the intensity, I, integrated over the Dalitz plot for a particular $K\pi\pi$ mass region equals the number of events for that particular $K\pi\pi$ mass region. For each $K\pi\pi$ mass region we define the integrated terms of equation (5), viz.,

$$\text{Number of events} = \sum_i X_{ii} + \sum_{i<j} \left(Y_{ij} + Z_{ij}\right), \quad (8)$$

wherein the X_{ii} are the number of events due to incoherent $K_V(890)\pi$ or $\rho(765)K$ and the Y_{ij} and Z_{ij} are the number of events associated with the real and imaginary parts of the off-diagonal interference terms.

Each Q mass band is fitted separately for $K^0\pi^0\pi^+$ and $K^+\pi^-\pi^+$. The Dalitz plots and corresponding mass plots are given in Figs. 18 to 20. For each mass band we perform maximum-likelihood fits. In the fits, Monte Carlo events are used to evaluate the normalization integrals. [44] They have the same selection as do the real events, $M(p\pi^+) > 1.5$ GeV.

(b) $K^0\pi^0\pi^+$ Dalitz plot fits. For $K^0\pi^0\pi^+$ we perform two incoherent fits to the diagonal density matrix elements -- fit no. 1 does not have the $K_V^0(890)$ and $K_V^+(890)$ couplings constrained to be equal while fit no. 2 does. Likewise we perform two fits to the entire density matrix -- fit no. 3 does not have the $K_V(890)$ couplings constrained to be equal while fit no. 4 does. The unconstrained fits are a test of whether the Q corresponds to an I = 1/2 state with branching ratios given by I-spin Clesbch-Gordan coefficients.

(The $K^0\pi^0\pi^+$ Dalitz-plot fits are to events without a t_{pp} cut. The few events with $-t_{pp} > 1$ GeV^2 do not appreciably change the Dalitz-plot distributions.) As is evident from the mass plots given in Fig. 19(a) and (b), there is for region I a greater amount of $K_V^+(890)$ than $K_V^0(890)$. The fitted d_{ij} values and the corresponding values of X, Y, and Z in Eq. (8) are given in Tables VIII and IX. The incoherent fits give fair qualitative fits, but fail in details (not shown). The fits to the entire density matrix are quantitatively better, as evidenced by the larger values of the logarithmic likelihood, the "ln w" entries in the tables. Differences in the "ln w" values can be interpreted as one-half times the differences in the chi-squares of the fits. The curves in Fig. 19 correspond to fit no. 4, the constrained fit to the entire density matrix. There is little difference between fits no. 3 and 4. In particular, the diagonal elements agree well, but the off-diagonal elements differ typically by a few standard deviations. For fit no. 3, Re d_{12} and Re d_{23} are in poor agreement for regions I and II.[45] This disagreement also indicates a larger amount of $K_V^+(890)$ than $K_V^0(890)$ for regions I and II.

There is a large $\rho(765)K$ contribution. For fit no. 2, the incoherent fit, the fraction of $\rho(765)K$ events (X_{22}/Total) has a constant value of about (0.35 ± 0.04). Since phase space increases with increasing $K\pi\pi$ mass in the Q region more rapidly for $\rho(765)K$ than for $K_V(890)\pi$, the corresponding coupling of $\rho(765)K$ relative to $K_V(890)\pi$ decreases with increasing $K\pi\pi$ mass. For fit no. 4, the ratios of d_{22}/d_{11} are for our four $K\pi\pi$ mass regions: (1.84 ± 0.44), (0.69 ± 0.13), (0.43 ± 0.06), and (0.36 ± 0.04).

(c) $K^+\pi^-\pi^+$ Dalitz-plot fits. For $K^+\pi^-\pi^+$, we perform in fit no. 5 incoherent fits to the diagonal elements of the density matrix, and in fit no. 6 we fit the entire density matrix. The incoherent fits are reasonable except for the $\pi^-\pi^+$ mass spectra (these fits are not shown). The entire density matrix fit reproduces better the $\pi\pi$ mass spectra. (See Tables X and XI.) The curves of Fig. 20 correspond to fit no. 6. For $K\pi\pi$ regions I and II, fit no. 6 yields smaller values of d_{22} (which is proportional to the $\rho(765)K$ coupling square) than does fit no. 5, due to about an 8% constructive interference effect. All other d_{ij} of both fits agree.

Except for region I, the incoherent amount of $K_V(890)\pi$ comprises approximately 75% of the Q. However, $K^+\pi^+$ misidentification spreads out the $K^+\pi^-$ mass spectrum and peaks the $\pi^-\pi^+$ mass spectrum at about 720 MeV. As discussed before, we estimate for the entire Q about 10% of the $K^+\pi^-\pi^+$ events have the K^+ and π^+ wrongly interchanged. Since we have not determined precisely this fraction for each separate $K^+\pi^-\pi^+$ mass region or the effects of misidentification upon the fits, we assume that the fitted amount of incoherent $K_V(890)\pi$ is actually 10% low due to this bias in order to estimate an upper bound on the actual amount of $K_V(890)\pi$. From our Monte Carlo study, there is some indication that this correction is too large for Region I. The errors for the corrected values do not include the uncertainty in the assumed fraction of 10%. Hence, the values quoted for $K_V(890)\pi$ could have systematic errors as large as 10%. We summarize the corrected values in Tables X and XI. The correction applied to the incoherent fits, fit no. 5, results in a $K_V(890)\pi$ fraction of about (0.82 ± 0.03) except for region I for which the correction gives (0.94 ± 0.03).

Analogously to the $K^0\pi^0\pi^+$ fitted d_{22} and d_{11} values, the $K^+\pi^-\pi^+$ fitted values (both the corrected and uncorrected values) also

have ratios of d_{22}/d_{11} decreasing for increasing $K\pi\pi$ mass except for the corrected values of mass region I (for which the correction is probably too large anyway).

(d) Comparison of Dalitz-plot fits. In comparing the $K^0\pi^0\pi^+$ and $K^+\pi^-\pi^+$ fits, we use fits no. 4 and 6 since interference effects are important. In Table XII we list the d_{ij} values corrected for the measurement efficiencies, the unseen K^0 decays, and the difference in confidence level cut-offs for the final states $pK^0\pi^0\pi^+$ and $pK^+\pi^-\pi^+$. There are three main points. First, for $K^+\pi^-\pi^+$ and for $K^0\pi^0\pi^+$ the d_{22} values (which correspond to $\rho(765)K$ corrected for $K^+\pi^+$ misidentification) are in reasonable agreement. For region I the uncorrected d_{22} value for $K^+\pi^-\pi^+$ agrees with the d_{22} value for $K^0\pi^0\pi^+$. Secondly, the differences in Re d_{12} and in Im d_{12} are not significant due to the large errors, except for the Re d_{12} values of regions I and II. Thirdly, there is a major disagreement in the d_{11} values. Both the corrected and uncorrected $K^+\pi^-\pi^+$ values of d_{11} which corresponds to $K_V(890)\pi$ are greater than the $K^0\pi^0\pi^+$ values, except for region II for which the values agree. Because of this disagreement it must be said that the fits disagree. Since an $\epsilon(700)K$ contribution is possible for $K^+\pi^-\pi^+$ but not for $K^0\pi^0\pi^+$, the $\epsilon(700)K$ hypothesis offers a possible simple cause for this disagreement. We do not attempt fits including $\epsilon(700)K$ because of the $K^+\pi^+$ misidentification complication.

(e) $\epsilon(700)K$ contribution. Independently of any $K^+\pi^-\pi^+$ fits, the $\epsilon(700)K$ contribution in $K^+\pi^-\pi^+$ is estimated by comparing the actual number of $K^+\pi^-\pi^+$ events with the expected number of $K_V(890)\pi$ and $\rho(765)K$ events. If the Q were pure $K_V(890)\pi$, $\rho(765)K$, or $\epsilon(700)K$, then the ratio of $K^0\pi^0\pi^+$ to $K^+\pi^-\pi^+$ events would be respectively 1, 2, or 0. For the four mass regions -- 1.1 to 1.2 GeV, 1.2 to 1.27 GeV, 1.27 to 1.36 GeV, and 1.36 to 1.46 GeV -- the ratios are (0.94 ± 0.07), (1.12 ± 0.07), (0.99 ± 0.06), and (0.93 ± 0.06). These ratios include corrections for the measurement efficiencies, unseen K^0 decays, and the different confidence level cut-offs. Since the $K^0\pi^0\pi^+$ fits demonstrate a significant $\rho(765)K$ contribution, the ratios imply the presence of additional $K^+\pi^-\pi^+$ events, which we attribute to $\epsilon(700)K$. By $\epsilon(700)$ we mean an I = 0 S-wave $\pi\pi$ state and not necessarily a resonance. Of course any $\epsilon(700)K$ contribution includes both incoherent $\epsilon(700)K$ and any interference with $K_V(890)\pi$ or $\rho(765)K$. The expected number of $K^+\pi^-\pi^+$ events is determined by a Monte Carlo integration of Eq. (5) with the density matrix elements obtained from $K^0\pi^0\pi^+$ fit no. 4 -- the fit to the entire density matrix with $K_V^+(890) = K_V^0(890)$. We attribute the difference between the actual and expected number of $K^+\pi^-\pi^+$ events as due to an $\epsilon(700)K$ contribution. We summarize our results in Table XIII. The estimated $\epsilon(700)K$ contributes to the $K^+\pi^-\pi^+$ events in our four $K\pi\pi$ mass regions the net fractions: (0.15 ± 0.10), (0.03 ± 0.08), (0.17 ± 0.06), and (0.22 ± 0.06).

IV. Discussion of Results

A. Summary of Results

We summarize our results and then compare them with the results obtained by three similar experiments. Our experimental results for the Q are:

(1) The $K^0\pi^0\pi^+$ mass spectrum has a two peak substructure with one peak at about 1260 MeV with a width of about 120 MeV and a second peak at about 1420 MeV with a width of about 80 MeV. The $K^+\pi^-\pi^+$ mass spectrum has a different shape without any dip at 1360 MeV. This difference may be due to the presence of an $\epsilon(700)K$ contribution to this final state. [By $\epsilon(700)$ we mean only an I = 0 S-wave $\pi\pi$ state.]

(2) The $K_N(1420)$ accounts for only about half of the second peak in the $K^0\pi^0\pi^+$ mass spectrum, which corresponds to a discrepancy of about 2.4 standard deviations.

(3) In agreement with the accepted Q I-spin of 1/2, the Q region of the final state $nK^0\pi^+\pi^+$ has a cross section of $(13 \pm 1)\mu b$, which corresponds to an $I = 3/2$ $K_V(890)\pi$ contribution to the Q of less than 2%.

(4) The Q is produced peripherally with the 1260-MeV $K\pi\pi$ mass region more peripherally produced than the 1420-MeV region.

(5) The Q decay-plane-normal spectra demonstrate that the Q is predominately in a spin-parity state of 1^+ with zero spin projection along the beam, $M_z = 0$. However, there are significant contributions of 0^- and/or 2^- and of spin states with $M_z \neq 0$. The $\langle Y_{20} \rangle$ moments of the Q decay-plane-normal are systematically smaller in absolute value for $K^0\pi^0\pi^+$ than those for $K^+\pi^-\pi^+$ in all four $K\pi\pi$ mass regions subdividing the Q. The $\langle \mathrm{Re}\ Y_{21} \rangle$ moments are non-zero.

(6) The $Q \to K_V(890)\pi^+$ and the $K_V(890) \to K^+\pi^-$ angular decay distributions imply the dominance of a 1^+ state which decays via S-wave into $K_V(890)\pi$.

(7) The Q consists predominately of $K_V(890)\pi$, but also of $\rho(765)K$. For the $K^0\pi^0\pi^+$ mode, the Q is about a third $\rho(765)K$, but interference effects are important. The ratio of $K^0\pi^0\pi^+$ to $K^+\pi^-\pi^+$ events is unity to within 6% for four Q mass subdivisions. Using the $K^0\pi^0\pi^+$ fitted parameters, we estimate the amount of $K_V(890)\pi$ and $\rho(765)K$ in $K^+\pi^-\pi^+$. We find an excess of $K^+\pi^-\pi^+$ events, which we suggest is due to an $\epsilon(700)K$ contribution in $K^+\pi^-\pi^+$.

B. Comparison with Other Experiments

Our experimental results are based upon an analysis of 30 163 events of 12 GeV/c $K^+p \to pK^+\pi^-\pi^+$, reaction (1); and 6431 events of $K^+p \to pK^0\pi^0\pi^+$, reaction (2). There are three similar K^+p experiments with an incident beam momentum near 12 GeV/c. First, the Lawrence Berkeley Laboratory, Trilling-Goldhaber Group (LBL-TG) have studied 7577 events of reaction (1) and 2272 events of reaction (2) at 9 GeV/c. Second, a collaboration of the Universities of Birmingham, Glasgow, and Oxford (BGO) have studied 7067 events of reaction (1) and 4232 events of reaction (2). Third, a group at the University of Rochester (UR) have studied 3463 events of reaction (1) and 828 events of reaction (2) at 12.7 GeV/c. We proceed to compare our results summarized in the previous section with each of these experiments.

1. $K\pi\pi$ Mass Spectra

LBL-TG observe a two-peak substructure for the combined events of reactions (1) and (2) -- their low peak has $M_L = (1260 \pm 10)$MeV, $\Gamma_L = (40 \pm 10)$ MeV and their high peak has $M_H = (1380 \pm 20)$ MeV, $\Gamma_H = (120 \pm 20)$ MeV [see Fig. 21(a)]. In our $K^+\pi^-\pi^+$ mass of Figs. 1 and 3, we observe a single-bin peak centered at 1265 MeV with a width of ~10 MeV, our resolution, but observe no dip. Our peak has a statistical significance of about 4 standard deviations. Since this peak corresponds to one bin out of 50 for the entire Q region, we do not consider it as strong evidence for narrow $K\pi\pi$ substructure.

In our $K^0\pi^0\pi^+$ mass spectrum, the peak at 1260 MeV has a width of about 120 MeV, which is significantly larger than (40 ± 10) MeV. These results are inconsistent unless there are two interfering resonances with different relative phases at the two beam momenta. Such a model has been suggested by Goldhaber.[46]

BGO observe a 3σ dip at 1310 MeV in reaction (1), see Fig. 21(c). If they assume a Deck background and two incoherent resonances, they obtain in a fit to their combined data [see Fig. 21(b)] resonant masses and widths of M_H = 1260 MeV, Γ_H = 100 MeV, and M_L = 1390 MeV, Γ_L = 140 MeV. But they state that their Kππ mass spectra are also consistent with no substructure.

The Kππ mass spectra that we observe are consistent with those observed by UR [see Fig. 21 (e) and (f)]. They parametrize their spectra as a single peak with M = (1260 ± 20) MeV, Γ = (180 ± 20) MeV, a small shoulder on the high-mass side of the Q peak, and a smooth background.

2. $K_N(1420)$ Contribution

Both LBL-TG and BGO find that the $K_N(1420)$ does not fully account for their high Q peaks. BGO find that subtraction of $K_N(1420)$ events reduces their Q_H peak to a shoulder, but does not eliminate it [see Fig. 21(b)]. To calculate their $K_N(1420)$ contributions in Kππ, they assume that $K_N(1420) \to K\pi\pi$ is dominated by $K_V(890)\pi$ and that the branching ratio Kππ/Kπ is approximately unity instead of the value (0.64 ± 0.11) which we used. They normalize the amount of $K_N(1420) \to K\pi\pi$ via the amount of $K_N(1420)$ in the reaction $K^+p \to pK^0\pi^+$. For their combined data, BGO find that the $K_N(1420)$ contributes 8 or 9% of the events in the 1.42 GeV Kππ mass region (1.36 to 1.46 GeV).

UR attribute the high-mass shoulder of their Q enhancement to the $K_N(1420)$. For the reaction $K^+p \to pK_N(1420)$, $K_N(1420) \to K^0\pi^+$, they obtain a cross section of (30 ± 7) μb with which our result of (31 ± 5) μb agrees. When they use the $K_N(1420)$ branching ratios given in the 1969 Review of Particle Properties, which agree with the ratios used by us to within the quoted errors, they obtain an estimated

$K_N(1420) \to K^+\pi^-\pi^+$ contribution of 13% in the 1420-MeV Kππ mass region. If instead they fix the $K_N(1420)$ mass and width at 1420 MeV and 100 MeV and vary the amount of $K_N(1420)$ along with the amount, mass, and width of a 1^+ resonance plus a fourth order polynomial to describe the background, then they obtain about 22% for the $K_N(1420)$ contribution in the 1420-MeV Kππ mass region.

In comparison, we estimate that the $K_N(1420)$ contributes to Kππ mass region IV, (1.36 to 1.46 GeV) about 15% and 9%, respectively, for reactions (1) and (2). Our estimated percentages are consistent with the value obtained by BGO. Likewise our $K^+\pi^-\pi^+$ estimate is consistent with the UR estimate based upon the $K_N(1420)$ branching ratios, but not upon their Kππ mass fit.

3. I Spin of Q

LBL-TG places an upper limit of 2% to an I = 3/2 $K_V(890)\pi$ contribution to the Q, with which we agree. UR places an upper limit of 7 μb for $Q^{++} \to K^0\pi^+\pi^+$ in the reaction $K^+p \to nK^0\pi^+\pi^+$, $K^0 \to \pi^-\pi^+$, to be compared with our value of (13 ± 1)μb.

4. t_{pp} Distributions

All three experiments find that the Q is peripherally produced. Fitting $e^{Bt_{pp}}$ to their combined data BGO find that B = (7.1 ± 0.2) GeV^{-2} for $1.2 < M(K\pi\pi) < 1.4$ GeV and that B does not depend upon M(Kππ) for a $M(K\pi\pi) < 1.4$ GeV, but that B = (5.8 ± 0.3) GeV^{-2} for $1.4 < M(K\pi\pi) < 1.5$ GeV. When we fit separately reactions (1) and (2), we find similar slopes and also find a decrease in B values with increasing Kππ mass.

5. Q Decay-Plane-Normal

Both BGO and UR find that the Q decay-plane-normal

distribution is predominantly but not entirely $\sin^2\theta$ corresponding to a Q spin-parity of 1^+ with $M_z = 0$ with respect to the beam. BGO find for the Q that only the $\langle Y_{20} \rangle$ moment is consistent with being non-zero. In contrast we find that in addition to $\langle Y_{20} \rangle$ also $\langle \mathrm{Re}\ Y_{21} \rangle$ is non-zero. This difference is explainable as being due to the larger statistical error in the BGO moments.[47] If the Q were purely diffractive then only spin states with $M_z = 0$ would be produced. We also observe systematically smaller absolute values of $\langle Y_{20} \rangle$ for $K^0\pi^0\pi^+$ than for $K^+\pi^-\pi^+$. This result suggests possibly different production processes for $pK^0\pi^0\pi^+$ and $pK^+\pi^-\pi^+$; possibly additional evidence for this may be seen in that our t_{pp} distributions for $Q \to K^+\pi^-\pi^+$ have somewhat steeper slopes than those for $Q \to K^0\pi^0\pi^+$.

6. Two-Body Decay of the Q

We confirm BGO's conclusion that the Q decays into $K_V(890)\pi$ by predominantly S-wave. However, because of background complications we felt that we could not entirely exclude a possible D-wave contribution.

7. Q Dalitz Plot

LBL-TG fit the entire Q Dalitz plot to S-wave 1^+ $K_V(890)\pi$ and $\rho(765)K$ for reactions (1) and (2) simultaneously and find that the Q decays predominantly into $K_V(890)\pi$ which interferes strongly with $\rho(765)K$. In addition they find that the ratio of $pK^0\pi^0\pi^+$ to $pK^+\pi^-\pi^+$ events in the Q equals one. For pure $K_V(890)\pi$, $\rho(765)K$, or $\epsilon\,(700)K$ the ratio would be respectively 1, 2, and 0. Since they find a significant $\rho(765)K$ contribution, they suggest an additional $\epsilon\,(700)K$ contribution in $K^+\pi^-\pi^+$ as one possible explanation of this discrepancy.

In their Dalitz plot fits to separate reactions (1) and (2), BGO include both $J^P = 1^+$ and 2^- and $\epsilon\,(700)K$ as well as $K_V(890)\pi$ and $\rho(765)K$ amplitudes in order to obtain agreement between their $\rho(765)K$ amplitudes of reaction (1) and reaction (2). (They also find agreement for $J^P = 1^+$ and 0^-.) Finally they state that their experimental values for $\langle Y_{20} \rangle$ and $\langle Y_{40} \rangle$ are inconsistent with the decay structure given by their Dalitz plot fits provided that the Q is produced only with 1^+ and 2^- with $M_z = 0$ (or with 1^+ and 0^- with $M_z = 0$ only). They conclude that either the Dalitz plot structure of a 2^- background is very different from their assumed form or that there is some production with $M_z \neq 0$.

UR obtain a good fit to their $K^+\pi^-\pi^+$ Dalitz plot with a 1^+ resonance decaying coherently into $K_V(890)\pi$ and $\rho(765)K$, a $K_N(1420)$ contribution about twice that expected upon the basis of the $K_N(1420)$ branching ratios, and lastly, a uniform background of about $(20 \pm 10)\%$ given by phase space. They do not fit $K^0\pi^0\pi^+$ because of their low statistics, but find the $K^+\pi^-\pi^+$ fitted parameters yield a good prediction for $K^0\pi^0\pi^+$.

Instead of attempting to include other spin-parities in our Dalitz-plot fits, we have performed fits to a density matrix corresponding to only S-wave 1^+ $K_V(890)\pi$ and $\rho(765)K$ amplitudes, and have obtained reasonable fits with this approximate model. We also find interference effects are important. Using our parameters determined from fits to reaction (2), we calculate the expected number of $K_V(890)\pi$ and $\rho(765)K$ events in $K^+\pi^-\pi^+$. There is an excess of $K^+\pi^-\pi^+$ events, which we suggest may be due to an $\epsilon\,(700)K$ contribution. However, due to the possible effects of other spin-parities, which we have neglected, we consider our $\epsilon\,(700)K$ estimates as approximate.

Both BGO and we find that the $\rho(765)K$ coupling relative to the $K_V(890)\pi$ coupling decreases with increasing $K\pi\pi$ mass between 1.1 and 1.5 GeV. This variation is additional support for Q substructure, though it could also be due to an interference effect of a resonance with background.

C. Conclusions

In conclusion, the above results demonstrate the complexity of the Q enhancement. A meaningful resonant parametrization is difficult due to the possible contributions of the spin-parity states 0^-, D-wave 1^+, 2^-, and 2^+ in addition to the dominant S-wave 1^+. Similarly, attempts at determining the relative amounts of $K_V(890)\pi$ and $\rho(765)K$ are dependent upon the assumed J^P states and the nature of any background to the dominant $K_V(890)\pi$ and $\rho(765)K$ contributions. The observed ratio of $K^0\pi^0\pi^+$ to $K^+\pi^-\pi^+$ of unity suggests the presence of an $\epsilon(700)K$ contribution in $K^+\pi^-\pi^+$, but its precise determination is even more difficult than that of the relative amounts of $K_V(890)\pi$ and $\rho(765)K$.

ACKNOWLEDGMENTS

We gratefully acknowledge the help we received from Norman M. Uyeda and Victor Waluch. We thank Joseph J. Murray for his work in beam design and construction, the Stanford Linear Accelerator 82-inch Bubble Chamber group for their assistance in data gathering, and the LBL Group A Scanning and Measuring group for their help in data reduction.

FOOTNOTE AND REFERENCES

*Work done under the auspices of the U.S. Atomic Energy Commission

1. Particle Data Group, Review of Particle Properties, Rev. Mod. Phys. 43 (2), Part II, S1 (1971).
2. R. Armenteros et al., Phys. Letters 9, 207 (1964); also J. Barash et al., Phys. Rev. 145, 1095 (1966).
3. D.J. Crennell, G.R. Kalbfeisch, K. W. Lai, J. M. Scarr, and T.G. Schumann, Phys. Rev. Letters 19, 44 (1967).
4. A. Astier et al., Nucl. Phys. B10, 65 (1969).
5. A. Bettini et al., Nuovo Cimento 62A, 1038 (1969).
6. S.P. Almeida et al., Phys. Letters 16, 184 (1965).
7. B.C. Shen et al., Phys. Rev. Letters 17, 726 (1966).
8. G. Bassompierre et al., Phys. Letters 26B, 30 (1967).
9. J. Berlinghieri et al., Phys. Rev. Letters 18, 1087 (1967).
10. W. deBaere et al., Nuovo Cimento 49A, 374 (1967)
11. J. Bartsch et al., Nucl. Phys. B8, 9 (1968).
12. F. Bomse et al., Phys. Rev. Letters 20, 1519 (1968).
13. D. Denegri et al., Phys. Rev. Letters 20, 1194 (1968).
14. G. Alexander, A. Firestone, G. Goldhaber, and D. Lissauer, Nucl. Phys. B13, 503 (1969); also G. Goldhaber, A. Firestone, and B. C. Shen, Phys. Rev. Letters 19, 972 (1967).
15. J. Andrews et al., Phys. Rev. Letters 22, 731 (1969).
16. D.C. Colley et al., Nuovo Cimento 59A, 519 (1969).
17. J. M. Bishop et al., Nucl. Phys. B9, 403 (1969)
18. A.R. Erwin, W.D. Walker, A.T. Goshaw, and A. Weinberg, Nucl. Phys. B9, 364 (1969).

19. J. Friedman, A Study of the Reactions $K^-p \to p\bar{K}^0\pi^-$, $K^-p \to p\bar{K}^0\pi^0\pi^-$, and $K^-p \to n\bar{K}^0\pi^+\pi^-$ from 2.1 to 2.7 GeV/c, Lawrence Radiation Laboratory Report UCRL-18860, Apr. 1969.
20. C. Y. Chien et al., Phys. Letters 29B, 433 (1969); also a Dalitz plot analysis is given in C. Y. Chien et al., Phys. Letters 28B, 143 (1968).
21. S. U. Chung, R. L. Eiser, N. F. Bali, and D. Lüers, Phys. Rev. 182, 1443 (1969).
22. B. Werner et al., Phys. Rev. 188, 2023 (1969).
23. G. S. Abrams et al., Phys. Rev. D1, 2433 (1970).
24. P. Antich et al., Nucl. Phys. B20, 201 (1970).
25. K. W. J. Barnham et al., Nucl. Phys. B25, 49 (1970).
26. M. G. Bowler, Phys. Letters 31B, 318 (1970).
27. M. S. Farber, T. Ferbel, P. F. Slattery, and H. Yuta, Phys. Rev. D1, 78 (1970).
28. A. Firestone, The Q Region of $K\pi\pi$ Mass, in Experimental Meson Spectroscopy, C. Baltay and A. Rosenfeld, Eds. (Columbia University Press, New York, 1970), p. 229. Our preliminary data were included in this review.
29. A. F. Garfinkel et al., Phys. Rev. Letters 26, 1505 (1971).
30. A description of the beam is given in S. Flatté, Manual for K82 Beam Watchers, Lawrence Berkeley Laboratory Group A Physics Note No. 646, Feb. 1968.
31. G. F. Chew and A. Pignotti, Phys. Rev. Letters 20, 1078 (1968).
32. S. Flatté, Experiment 30(K82) Scanning Instructions, Lawrence Berkeley Laboratory Group A Physics Note No. 637 Rev., Feb. 1968.

33. Stephen E. Derenzo and Roger H. Hildebrand, Nucl. Instr. Methods 69, 287 (1969).

34. P. Davis and S. Flatté, K82 Path Length Determination, Lawrence Berkeley Laboratory Group A Physics Note No. 700, Jan. 1970.

35. Philip J. Davis and Stanley M. Flatté, K82 Measurement Efficiencies for Event Types 4 and 12, Lawrence Berkeley Laboratory Group A Physics Note. No. 724, Feb. 1971.

36. J.S. Danburg and G.R. Lynch, BUBBLE, A Program to Utilize Spiral Reader Measurements of Track Brightness, Lawrence Berkeley Laboratory Group A Programming Note. No. P-160 Rev., May 1967.

37. For the Monte Carlo events the best fit is defined as the one with minimum kinematic chi-square since the pulse heights corresponding to Spiral Reader measurements are not simulated. There is negligible difference in bubble-density chi-square for real ambiguous events in the Q region.
In our Monte Carlo generation, we use a version of PHONY modified by Norm Uyeda to use a more efficient program in the generation of four-momenta, SAGE. See references 38 to 40.

38. Philip Davis, K82 Version of PHONY, Lawrence Berkeley Laboratory Group A Physics Note No. 184, March 1969.

39. E. Burns and D. Drijard, PHONY, Lawrence Berkeley Laboratory Trilling-Goldhaber Group Technical Note. No. 143, 1968.

40. Jerome H. Friedman, J. Comput. Phys. 7, 201 (1971); see also, Jerry Friedman, SAGE, A General System for Monte Carlo Event Generation with Preferred Phase Space Density Distributions,

Lawrence Berkeley Laboratory Group A Programming Note No. P-189 Rev., Jan. 1971.

41. Our $K_V(890)$ and $\rho(765)$ selections are respectively $0.84 < M(K\pi) < 0.94$ GeV and $0.65 < M(\pi\pi) < 0.85$ GeV.

42. Philip J. Davis, Stephen E. Derenzo, Stanley M. Flatté, Margaret A. Garnjost, Gerald R. Lynch, and Frank T. Solmitz, Phys. Rev. Letters 23, 1071 (1969).

43. Motivated by the structure of the $K^0\pi^0\pi^+$ mass spectrum, we subdivide the Q into four $K\pi\pi$ mass regions: (I) 1.1 to 1.2 GeV, (II) 1.2 to 1.27 GeV, (III) 1.27 to 1.36 GeV, and (IV) 1.36 to 1.46 GeV.

44. We make a linear approximation to the $K\pi\pi$ mass spectrum in the integrations. A description of the program we used is given in Philippe H. Eberhard and Werner O. Koellner, The Optime System for Fitting Theoretical Expressions, Lawrence Radiation Laboratory Report UCRL-20159, Oct. 1970.

45. The indices correspond to $K_V(890)\pi^+$, $\rho(765)K$, and $K_V(890)\pi^0$ for values of 1, 2, and 3.

46. Gerson Goldhaber, K^* Spectrum and Diffraction Dissociation Effects (including A_1), in Meson Spectroscopy, Charles Baltay and Arthur H. Rosenfeld, Eds. (W. A. Benjamin, Inc.) New York, 1968).

47. In the reaction $K^-p \to Q^-p$ at 10 GeV/c, the Aachen-Berlin-Bonn-CERN-Cracow-Heidelberg-London-Vienna Collaboration, Phys. Letters 34B, 160 (1971), found $\langle \mathrm{Re}\, Y_{21} \rangle$ consistent with zero in the reference frame we use, with about the same statistical error as in our experiment. This was taken as evidence for t-channel helicity conservation in a $\Delta J = 1$, diffractive process.

Table I. Summary of data reduction.

	Four-prongs	Vee two-prongs
No. of events	189 000	38 000
First-scan efficiency	0.97	0.91
Double-scan efficiency	1.00	0.99
First-measurement efficiency	0.738 ± .008	0.67 ± .02
Net measurement efficiency[a]	0.897 ± .013	0.846 ± .026

[a] The fraction of events passing, after at least two measurements of all failing events and three measurements for half of the twice-failing events.

Table II. Cross sections for 12 GeV/c K^+p.

Reaction	No. events	Cross section (μb)
(1) $K^+p \to pK^+\pi^-\pi^+$		
No cuts	30163	935 ± 30
$M(K\pi\pi) < 1.5$ GeV	8961	278 ± 9
$M(K\pi\pi) < 1.5$ GeV, $M(p\pi^+) > 1.5$ GeV, $-t_{pp} < 1$ GeV^2	7687	238 ± 8
(2) $K^+p \to pK^0\pi^0\pi^+$		
No cuts	6431	650 ± 28
$M(K\pi\pi) < 1.5$ GeV	2283	231 ± 11
$M(K\pi\pi) < 1.5$ GeV, $M(p\pi^+) > 1.5$ GeV, $-t_{pp} < 1$ GeV^2	1919	194 ± 9
(3) $K^+p \to nK^0\pi^+\pi^+$		
No cuts	1279	129 ± 6
$M(K\pi\pi) < 1.5$ GeV, $-t_{pn} < 1$ GeV^2	126	13 ± 1
(4) $K^+p \to pK^0\pi^+$		
No cuts	1900	246 ± 11

Table III. Fit-ambiguity results for Q events.[a]

A. Best fit to $pK^+\pi^-\pi^+$	Percent with 2nd best fit to: $pK^+\pi^-\pi^+$[b]	$pK^+K^-K^+$	$pK^+\bar{p}p$	Total
Without χ^2_{BD} selection	40%	3%	4%	47%
With χ^2_{BD} selection[c]	40	1	2	43

B. Best fit to $pK^0\pi^0\pi^+$	Percent with 2nd best fit to $pK^0K^0K^+$	$nK^0K^+K^+$	Total
With χ^2_{BD} selection[c]	3%	5%	9%

[a] The Q selection is $M(K\pi\pi) < 1.5$ GeV and $M(p\pi^+) > 1.5$ GeV.

[b] For $pK^+\pi^-\pi^+$ vs. $pK^+\pi^-\pi^+$, the 40% corresponds to permutation ambiguities.

[c] The bubble-density χ^2 selection is that the χ^2_{BD} be less than five plus the minimum χ^2_{BD} of all fits.

Table IV. FWHM resolutions for $K\pi\pi$ mass less than 1.5 GeV and $p\pi^+$ mass greater than 1.5 GeV.

Mass	Γ_{FWHM} (MeV)
$K^+\pi^-\pi^+$	13.0
$K^+\pi^-$	8.6
$\pi^+\pi^-$	8.0
$K^0\pi^0\pi^+$	25.6
$K^0\pi^0$	20.0
$K^0\pi^+$	9.4
$\pi^0\pi^+$	23.7

Table V. Two-body $K_N(1420)$ fits

A. $K^0\pi^+$ mass-plot fit over the range 1200 to 1650 MeV in 10-MeV bins.

1420 mass, m_R	1420 ± 10 MeV
1420 width, Γ_R	$136 \pm {}^{42}_{30}$ MeV
Background slope, s	-.65 ± .4
Signal to signal plus background ratio, r	.81 ± .07
Fit χ^2	48.5
Confidence level, CL	.14

B. Fits of $Ae^{Bt_{pp}}$ to t_{pp} plots from 0.0 to 0.4 GeV^2 in 0.1-GeV^2 bins.

$K\pi$ mass interval		A (events/GeV^2)	B(GeV^{-2})	CL
(i)	1.2 to 1.35 GeV	$43 \pm {}^{9}_{8}$	4.0 ± 1	.51
(ii)	1.35 to 1.50 GeV	$49 \pm {}^{9}_{7}$	2.3 ± .8	.31
(iii)	1.50 to 1.65 GeV	$22 \pm {}^{7}_{5}$	2.8 ± 1.4	.44

Table VI. Fits of $Ae^{Bt_{pp}}$ to t_{pp} spectra of $K\pi\pi$

M($K\pi\pi$) region (GeV)	A in events/GeV^2 $pK^+\pi^-\pi^+$ [a]	A in events/GeV^2 $pK^0\pi^0\pi^+$ [b]	B in GeV^{-2} (confidence level) $pK^+\pi^-\pi^+$ [a]	B in GeV^{-2} (confidence level) $pK^0\pi^0\pi^+$ [b]
(I) 1.1 to 1.2	568 ± 27	278 ± 27	9.5 ± .4(5.2×10^{-1})	8.3 ± .6(8.1×10^{-1})
(II) 1.2 to 1.27	688 ± 29	394 ± 32	9.0 ± .3(3.6×10^{-3})	7.9 ± .5(1.6×10^{-2})
(III) 1.27 to 1.36	784 ± 29	410 ± 31	7.6 ± .3(9.7×10^{-2})	6.9 ± .5(2.6×10^{-1})
(IV) 1.36 to 1.46	644 ± 25	323 ± 25	6.5 ± .2(1.2×10^{-4})	6.1 ± .5(5.7×10^{-1})
entire Q	3014 ± 57	743 ± 27 [a]	7.9 ± .1(1.8×10^{-9})	6.9 ± .5(7.7×10^{-2}) [a]

[a] Fits are to t_{pp} from 0.0 to 0.4 GeV^2 in 0.05-GeV^2 bins.

[b] Fits are to t_{pp} from 0.0 to 0.4 GeV^2 in 0.1 -GeV^2 bins.

Table VII. Selected Q decay-plane-normal moments.

	$K\pi\pi$ mass region (GeV)			
	I (1.1 to 1.2)	II (1.2 to 1.27)	III (1.27 ± 1.36)	IV (1.36 to 1.46)
$\langle Y_{20} \rangle$				
$K^+\pi^-\pi^+$	-.087 ± .008	-.099 ± .006	-.087 ± .006	-.082 ± .006
$K^0\pi^0\pi^+$	-.059 ± .017	-.062 ± .011	-.073 ± .011	-.056 ± .011
$\langle \mathrm{Re}\, Y_{21} \rangle$				
$K^+\pi^-\pi^+$	-.025 ± .006	-.017 ± .006	-.011 ± .003	-.006 ± .03
$K^0\pi^0\pi^+$	-.028 ± .011	-.023 ± .008	-.006 ± .008	-.020 ± .008
$\langle Y_{40} \rangle$				
$K^+\pi^-\pi^+$	-.005 ± .007	-.002 ± .006	+.005 ± .006	.005 ± .006
$K^0\pi^0\pi^+$	-.020 ± .015	-.018 ± .014	-.009 ± .011	+.008 ± .013
$\langle \mathrm{Re}\, Y_{43} \rangle$				
$K^+\pi^-\pi^+$	+.012 ± .006	-.012 ± .006	-.010 ± .004	-.004 ± .005
$K^0\pi^0\pi^+$	.000 ± .013	-.004 ± .010	-.012 ± .009	+.011 ± .009

Table VIII. $K^0\pi^0\pi^+$ incoherent Dalitz plot fits.

Fit. No. 1

$M(K\pi\pi)$ region (GeV)	Density matrix elements[a]				Number of events[b]			
	d_{11}	d_{22}	d_{33}	X_{11}	X_{22}	X_{33}	Total	ln w[c]
(I) 1.1 to 1.2	85 ± 13	308 ± 47	113 ± 14	92 ± 14	113 ± 17	129 ± 17	334 ± 18	1668.6
(II) 1.2 to 1.27	137 ± 20	182 ± 22	171 ± 20	141 ± 21	179 ± 22	190 ± 23	509 ± 23	2799.4
(III) 1.27 to 1.36	214 ± 25	115 ± 12	188 ± 23	198 ± 23	227 ± 24	179 ± 2	604 ± 25	3508.2
(IV) 1.36 to 1.46	231 ± 25	76 ± 8	214 ± 24	183 ± 20	195 ± 21	173 ± 20	550 ± 23	3072.2

Fit No. 2

$M(K\pi\pi)$ region (GeV)	Density matrix elements			Number of events[b]			
	$d_{11} = d_{33}$	d_{22}	X_{11}	X_{22}	X_{33}	Total	ln w
(I) 1.1 to 1.2	99 ± 9	311 ± 47	107 ± 10	114 ± 17	113 ± 11	334 ± 18	1667.4
(II) 1.2 to 1.27	154 ± 12	182 ± 22	159 ± 12	179 ± 22	171 ± 13	509 ± 23	2798.8
(III) 1.27 to 1.36	201 ± 15	115 ± 12	186 ± 14	227 ± 24	192 ± 14	604 ± 25	3508.0
(IV) 1.36 to 1.46	222 ± 16	76 ± 8	176 ± 12	195 ± 21	179 ± 13	550 ± 23	3072.1

[a] The density matrix elements, d_{ij}, are proportional to products of the $K_V(890)\pi$ and/or $\rho(765)K$ couplings. The indices correspond to $K^0_V(890)\pi^+$, $\rho(765)K$, and $K^+_V(890)\pi^0$ for values of 1, 2, and 3.

[b] The X_{ii} are the corresponding number of events defined by Eq. (8).

[c] The ln w are the logarithmic likelihoods as defined in Ref. 44.

Table IX. $K^0\pi^0\pi^+$ Dalitz plot fits to the entire density matrix.

Fit No. 3[a]

Density matrix elements

M(Kππ) region (GeV)		d_{11}	d_{22}	d_{33}	Re d_{12}	Im d_{12}	Re d_{13}	Im d_{13}	Re d_{23}	Im d_{23}	ln w
(I)	1.1 to 1.2	95 ± 26	245 ± 55	149 ± 26	-13 ± 32	61 ± 67	122 ± 21	72 ± 32	142 ± 29	70 ± 20	1697.4
(II)	1.2 to 1.27	181 ± 31	113 ± 23	195 ± 29	22 ± 28	19 ± 39	251 ± 25	7 ± 28	90 ± 29	-4 ± 40	2856.4
(III)	1.27 to 1.36	193 ± 42	91 ± 12	231 ± 43	76 ± 25	-19 ± 24	192 ± 31	-57 ± 100	22 ± 23	-6 ± 24	3530.1
(IV)	1.36 to 1.46	262 ± 39	79 ± 10	184 ± 38	10 ± 27	37 ± 28	131 ± 47	124 ± 134	3 ± 27	18 ± 28	3079.6

Number of events

M(Kππ) region (GeV)		X_{11}	X_{22}	X_{33}	Y_{12}	Z_{12}	Y_{13}	Z_{13}	Y_{23}	Z_{23}	Total
(I)	1.1 to 1.2	103 ± 28	90 ± 20	170 ± 30	-2 ± 6	-16 ± 18	-13 ± 2	1 ± 0	23 ± 5	-21 ± 6	334 ± 18
(II)	1.2 to 1.27	187 ± 32	111 ± 22	216 ± 32	-6 ± 7	- 6 ± 12	-29 ± 3	0 ± 1	23 ± 7	2 ± 1	509 ± 23
(III)	1.27 to 1.36	178 ± 39	180 ± 24	220 ± 41	23 ± 7	5 ± 6	-12 ± 2	0 ± 1	7 ± 8	2 ± 8	604 ± 25
(IV)	1.36 to 1.46	208 ± 31	203 ± 25	148 ± 30	3 ± 8	- 4 ± 3	- 1 ± 3	1 ± 1	1 ± 9	-3 ± 4	550 ± 23

Fit No. 4

Density matrix elements

M(Kππ) region (GeV)		$d_{11} = d_{33} =$ Re d_{13}	d_{22}	Re d_{12} = Re d_{23}	Im d_{12} = Im d_{23}	Re d_{13}	Im d_{13} = 0	ln w
(I)	1.1 to 1.2	123 ± 14	226 ± 54	67 ± 20	60 ± 43	123 ± 14	0	1684.9
(II)	1.2 to 1.27	183 ± 16	126 ± 23	56 ± 19	16 ± 26	183 ± 16	0	2847.3
(III)	1.27 to 1.36	213 ± 15	91 ± 12	48 ± 17	-13 ± 16	213 ± 15	0	3527.5
(IV)	1.36 to 1.46	224 ± 16	80 ± 10	8 ± 20	22 ± 23	224 ± 16	0	3074.3

Number of events

M(Kππ) region (GeV)		X_{11}	X_{22}	X_{33}	Y_{12}	Z_{12}	Y_{13}	Z_{13}	Y_{23}	Z_{23}	Total
(I)	1.1 to 1.2	133 ± 15	83 ± 20	141 ± 16	12 ± 4	-16 ± 12	-13 ± 1	0	11 ± 3	-18 ± 13	334 ± 18
(II)	1.2 to 1.27	189 ± 16	124 ± 23	203 ± 17	14 ± 5	- 5 ± 8	-21 ± 2	0	13 ± 5	- 6 ± 10	509 ± 23
(III)	1.27 to 1.36	197 ± 14	180 ± 24	203 ± 14	14 ± 5	3 ± 4	-14 ± 1	0	16 ± 6	4 ± 5	604 ± 25
(IV)	1.36 to 1.46	178 ± 13	205 ± 25	181 ± 13	2 ± 6	- 3 ± 3	-13 ± 1	0	3 ± 6	- 3 ± 3	550 ± 23

[a] See footnotes in Table VIII.

Table X. $K^+\pi^-\pi^+$ incoherent Dalitz plot fits.

Fit. No. 5[a]

M(Kππ) region (GeV)		Density matrix elements d_{11}	d_{22}	Number of events X_{11}	X_{22}	Total	ln w
(I)	1.1 to 1.2	464 ± 16	915 ± 97	999 ± 34	174 ± 18	1172 ± 34	7748.3
(II)	1.2 to 1.27	545 ± 19	785 ± 51	1099 ± 37	404 ± 26	1504 ± 39	10 318.7
(III)	1.27 to 1.36	798 ± 24	518 ± 32	1489 ± 45	533 ± 33	2023 ± 45	14 345.1
(IV)	1.36 to 1.46	937 ± 28	355 ± 24	1501 ± 45	455 ± 44	1956 ± 44	13 743.5

Fit No. 5 corrected[b]

M(Kππ) region (GeV)		Density matrix elements d_{11}	d_{22}	Number of events X_{11}	X_{22}	Total
(I)	1.1 to 1.2	516 ± 18	331 ± 100	1110 ± 38	63 ± 19	1172 ± 34
(II)	1.2 to 1.27	606 ± 21	548 ± 52	1221 ± 41	282 ± 27	1504 ± 39
(III)	1.27 to 1.36	887 ± 27	357 ± 33	1655 ± 51	368 ± 34	2023 ± 45
(IV)	1.36 to 1.46	1041 ± 31	226 ± 24	1668 ± 50	288 ± 31	1956 ± 44

[a] See footnotes in Table VIII.

[b] We estimate a correction for $K^+\pi^+$ misidentification by increasing X_{11} by 10% and recalculating X_{22}, d_{11}, and d_{22}. The errors do not include possible systematic errors.

Table XI. $K^+\pi^-\pi^+$ Dalitz plot fits to the entire density matrix

Fit No. 6[a]

M(Kππ) region (GeV)	Density matrix elements d_{11}	d_{22}	Re d_{12}	Im d_{12}	Number of events X_{11}	X_{22}	Y_{12}	Z_{12}	Total	ln w
(I) 1.1 to 1.2	466 ± 24	520 ± 95	442 ± 65	27 ± 133	1003 ± 52	99 ± 18	79 ± 12	-7 ± 36	1172 ± 34	7772.4
(II) 1.2 to 1.27	525 ± 23	614 ± 50	410 ± 48	-91 ± 71	1059 ± 45	316 ± 26	102 ± 12	27 ± 21	1504 ± 39	10354.9
(III) 1.27 to 1.36	805 ± 26	502 ± 33	93 ± 39	100 ± 40	1503 ± 48	517 ± 34	31 ± 13	-28 ± 11	2023 ± 45	14353.5
(IV) 1.36 to 1.46	946 ± 29	346 ± 25	-40 ± 40	61 ± 40	1515 ± 46	443 ± 32	10 ± 10	7 ± 5	1956 ± 44	13745.1

Fit No. 6 corrected[b]

M(Kππ) region (GeV)	Density matrix elements d_{11}	d_{22}	Number of events X_{11}	X_{22}	Total
(I) 1.1 to 1.2	518 ± 27	-66 ± 100	1115 ± 58	-13 ± 19	1172 ± 34
(II) 1.2 to 1.27	583 ± 25	386 ± 52	1176 ± 51	199 ± 27	1504 ± 39
(III) 1.27 to 1.36	894 ± 29	340 ± 33	1669 ± 54	350 ± 34	2023 ± 45
(IV) 1.36 to 1.46	1051 ± 32	215 ± 25	1684 ± 51	275 ± 32	1956 ± 44

[a] See footnotes in Table VIII.

[b] See footnote b in Table X.

Table XII. Comparison of Kππ Dalitz plot fits.

	Kππ mass region (GeV) I (1.1 to 1.2)	II (1.2 to 1.36)	III (1.36 to 1.46)	IV (1.36 to 1.46)
Density matrix element d_{11}[a]				
$K^0\pi^0\pi^+$, fit 4	453 ± 51	673 ± 57	784 ± 56	824 ± 59
$K^+\pi^-\pi^+$, fit 6	520 ± 27	585 ± 25	897 ± 29	1055 ± 32
Fit 6 corrected[b]	577 ± 30	650 ± 29	997 ±32	1172 ± 36
Density matrix element d_{22}[a]				
$K^0\pi^0\pi^+$, fit 4	832 ± 200	464 ± 85	335 ± 45	294 ± 36
$K^+\pi^-\pi^+$, fit 6	580 ± 105	685 ± 56	560 ± 36	386 ± 27
Fit 6 corrected[b]	-74 ± 111	430 ± 60	379 ± 37	240 ± 29
Density matrix element Re d_{12}[a]				
$K^0\pi^0\pi^+$, fit 4	247 ± 75	206 ± 69	177 ± 63	29 ± 75
$K^+\pi^-\pi^+$, fit 6	493 ± 73	457 ± 53	104 ± 44	-45 ± 44
Density matrix element Im d_{12}[a]				
$K^0\pi^0\pi^+$, fit 4	221 ± 158	59 ± 96	-48 ± 59	81 ± 83
$K^+\pi^-\pi^+$, fit 6	30 ± 148	-101 ± 79	111 ± 44	-68 ± 45

[a] These entries are corrected for the measurement efficiencies and unseen K^0's.

[b] See footnote b of Table X.

Table XIII. Comparison of total number of Q events per $K\pi\pi$ mass region.

	$K\pi\pi$ mass region (GeV)			
	I (1.1 to 1.2)	II (1.2 to 1.27)	III (1.27 to 1.36)	IV (1.36 to 1.46)
$K^0\pi^0\pi^+$ observed	334 ± 18	509 ± 23	604 ± 25	550 ± 23
$K^0\pi^0\pi^+$ corrected[a]	1228 ± 77	1 874 ± 101	2222 ± 113	2025 ± 106
$K^+\pi^-\pi^+$ observed	1172 ± 34	1504 ± 39	2023 ± 45	1956 ± 44
$K^+\pi^-\pi^+$ corrected[a]	1307 ± 43	1677 ± 50	2255 ± 60	2181 ± 59
Ratio of $K^0\pi^0\pi^+/K^+\pi^-\pi^+$[a]	0.94 ± .07	1.12 ± .07	0.99 ± .06	0.93 ± .06
$K^+\pi^-\pi^+$ expected[b]	1117 ± 129	1631 ± 129	1880 ± 117	1696 ± 110
Actual minus expected	190 ± 136	46 ± 132	376 ± 132	485 ± 125

[a] These entries are corrected for the measurement efficiencies and unseen K^0's.

[b] The expected number of $K^+\pi^-\pi^+$ events is calculated using the d_{ij} values obtained from $K^0\pi^0\pi^+$ fit no. 4.

FIGURE CAPTIONS

Fig. 1. The $K\pi\pi$ mass spectra with no cuts for $K^+p \to pK^+\pi^-\pi^+$ and $pK^0\pi^0\pi^+$. The shaded areas are the estimated $K_N(1420)$ contributions of 360 and 140 events in $K^+\pi^-\pi^+$ and $K^0\pi^0\pi^+$. The line is our estimation for $K^0\pi^0\pi^+$ of the background in the 1420-MeV region.

Fig. 2. The missing-mass square for the hypotheses $K^+p \to pK^0\pi^+$(MM) and $K^0\pi^+\pi^+$(MM) in (a) and (b), respectively, for events with p_p^{Lab} or $p_{(MM)}^{Lab}$ less than 1 GeV/c. For (b) there is an additional selection on $M(K\pi\pi) < 1.5$ GeV. The shaded areas correspond, respectively to events with best fits to $pK^0\pi^+\pi^0$ and $K^0\pi^+\pi^+n$. Figures (a) and (b) correspond to subsamples of, respectively, 25% and 90% of all vee two-prongs.

Fig. 3. The $K^+\pi^-\pi^+$ and $K^0\pi^0\pi^+$ mass spectra: (a, b) for $M(p\pi^+) > 1.5$ GeV and $-t_{pp} < 1$ GeV^2; (c, d) for also $K_V(890)$ or $\rho(765)$; and (e, f) for $K_V(890)$.[41] The shaded areas correspond to $K^+\pi^-\pi^+$ events with a permutation ambiguity.

Fig. 4. The $K\pi\pi$ mass for Q events in $K^+p \to pK^+\pi^-\pi^+$ and $pK^0\pi^0\pi^+$: (a, b) are for $-t_{pp} < 0.1$ GeV^2; (c, d) are for $0.1 < -t_{pp} < 0.3$ GeV^2; (e, f) are for $-t_{pp} > 0.3$ GeV^2.

Fig. 5. The $K\pi\pi$ mass spectrum for $K^+p \to nK^0\pi^+\pi^+$ for events with $-t_{pn} < 1$ GeV^2.

Fig. 6. The $K\pi$ mass spectrum in the 1.42-GeV region for $K^+p \to pK^0\pi^+$. The curve corresponds to a fit of the mass and width of the $K_N(1420)$, the amount of $K_N(1420)$, and a linear background as given in Table V.

Fig. 7. The t_{pp} spectra for Q events in $K^+p \to pK^+\pi^-\pi^+$, the □'s; and in $K^+p \to pK^0\pi^0\pi^+$, the ▲'s.

Fig. 8. The t_{pp} spectra for Q events in $K^+p \to pK^+\pi^-\pi^+$ plotted in 0.05-GeV^2 bins, the □'s; and in $K^+p \to pK^0\pi^0\pi^+$ plotted in 0.1-GeV^2 bins, the ▲'s. (a, . . . , d) correspond to Kππ mass regions: (I) 1.1 to 1.2 GeV, (II) 1.2 to 1.27 GeV, (III) 1.27 to 1.36 GeV, and (IV) 1.36 to 1.46 GeV.

Fig. 9. The t_{pp} spectra for $K^+p \to pK^0\pi^+$ plotted in 0.1-GeV^2 bins for $K^0\pi^+$ mass intervals: (i) 1.2 to 1.35 GeV, the □'s; (ii) 1.35 to 1.50 GeV, the ♦'s; and (iii) 1.50 to 1.65 GeV, the ▲'s.

Fig. 10. In (a) and (b) the t_{pp} spectra of $K^+p \to pK^+\pi^-\pi^+$, □, in 0.05-GeV^2 bins and $K^+p \to pK^0\pi^0\pi^+$, ▲, in 0.1-GeV^2 bins both for $1.36 < M(K\pi\pi) < 1.46$ GeV. The ♦ points are the estimated $K_N(1420)$ contributions.

Fig. 11. The Q decay-plane-normal projection upon the beam for $K^+p \to pK^+\pi^-\pi^+$ and $pK^0\pi^0\pi^+$. (a, b), . . . , (g, h) are for Q mass regions--(I) 1.1 to 1.2 GeV, (II) 1.2 to 1.27 GeV, (III) 1.27 to 1.36 GeV, and (IV) 1.36 to 1.46 GeV. The shaded areas correspond to $K^+\pi^-\pi^+$ events with a permutation ambiguity.

Fig. 12. The Φ distributions of the Q decay-plane-normal for $K^+p \to pK^+\pi^-\pi^+$ and $pK^0\pi^0\pi^+$. (a, b), . . . , (g, h) are for Q mass regions--(I) 1.1 to 1.2 GeV, (II) 1.2 to 1.27 GeV, (III) 1.27 to 1.36 GeV, and (IV) 1.36 to 1.46 GeV. The shaded areas correspond to $K^+\pi^-\pi^+$ events with a permutation ambiguity. The z - and y-axes are defined in the Q rest frame as along the beam and the production-plane-normal.

Fig. 13. The angular distributions of $Q \to K_V(890)\pi$ for $K^+p \to pK^+\pi^-\pi^+$ with $K_V(890)$ selection, where (a, b), . . . , (g, h) are for Q mass regions-- (I) 1.1 to 1.2 GeV, (II) 1.2 to 1.27 GeV, (III) 1.27 to 1.36 GeV, and (IV) 1.36 to 1.46 GeV.[41] The shaded areas correspond to events with a permutation ambiguity.

Fig. 14. The $K_V(890)$ angular-decay spectra with axes in the Kππ rest frame. (a, b), . . . , (g, h) are for $K^+\pi^-\pi^+$ events in the Q mass regions--(I) 1.1 to 1.2 GeV, (II) 1.2 to 1.27 GeV, (III) 1.27 to 1.36 GeV, and (IV) 1.36 to 1.46 GeV.[41] The shaded areas correspond to events with a permutation ambiguity.

Fig. 15. The Q Dalitz plots--in (a) $M^2(\pi^-\pi^+)$ vs $M^2(K^+\pi^-)$ for $K^+\pi^-\pi^+$ and in (b) $M^2(K^0\pi^+)$ vs $M^2(K^0\pi^0)$ for $K^0\pi^0\pi^+$. The curves correspond to boundaries for a $M(K\pi\pi) = 1.32$ GeV.

Fig. 16. Kπ mass spectra with a $K_V(890)$ possible: $K^+\pi^-$ for $K^+p \to pK^+\pi^-\pi^+$ in (a); $K^0\pi^0$ and $K^0\pi^+$ for $K^+p \to pK^0\pi^0\pi^+$ in (b) and (c). The shaded area in (a) corresponds to events with a permutation ambiguity.

Fig. 17. The ππ mass spectra for Q events in (a) $K^+p \to pK^+\pi^-\pi^+$ and (b) $pK^0\pi^0\pi^+$. In (a) the shaded area corresponds to events with a permutation ambiguity.

Fig. 18. Dalitz plots for $K^+\pi^-\pi^+$ and $K^0\pi^0\pi^+$ where (a, b), . . . , (g, h) are for Q mass regions: (I) 1.1 to 1.2 GeV, (II) 1.2 to 1.27 GeV, (III) 1.27 to 1.36 GeV, and (IV) 1.36 to 1.46 GeV. The curves correspond to boundaries for Kππ masses of (I) 1.15 GeV, (II) 1.24 GeV, (III) 1.32 GeV, and (IV) 1.42 GeV.

Fig. 19. The $K^0\pi^0$, $K^0\pi^+$, and $\pi^0\pi^+$ mass spectra of $K^+p \to pK^0\pi^0\pi^+$ where (a, b, c), . . . , (j, k, l) are for Q mass regions--(I) 1.1 to 1.2 GeV, (II) 1.2 to 1.27 GeV, (III) 1.27 to 1.36 GeV, and (IV) 1.36 to 1.46 GeV. The curves correspond to the density matrix fits described in the text (fit no. 4 of Table IX).

Fig. 20. The $K^+\pi^-$, $K^+\pi^+$, and $\pi^-\pi^+$ mass spectra of $K^+p \to pK^+\pi^-\pi^+$ where (a, b, c), . . . , (j, k, l) are for Q mass regions--(I) 1.1 to 1.2 GeV, (II) 1.2 to 1.27 GeV, (III) 1.27 to 1.36 GeV, and (IV) 1.36 to

1.46 GeV. The curves correspond to density matrix fits described in the text (fit no. 6 of Table XI).

Fig. 21. The $K\pi\pi$ spectra observed by three other K^+p experiments: LBL-TG in (a), Ref. 14; BGO in (b) to (d), Ref. 25; UR in (e) and (f), Ref. 27. The shaded areas correspond to events without $\Delta^{++}(1236)$ present.

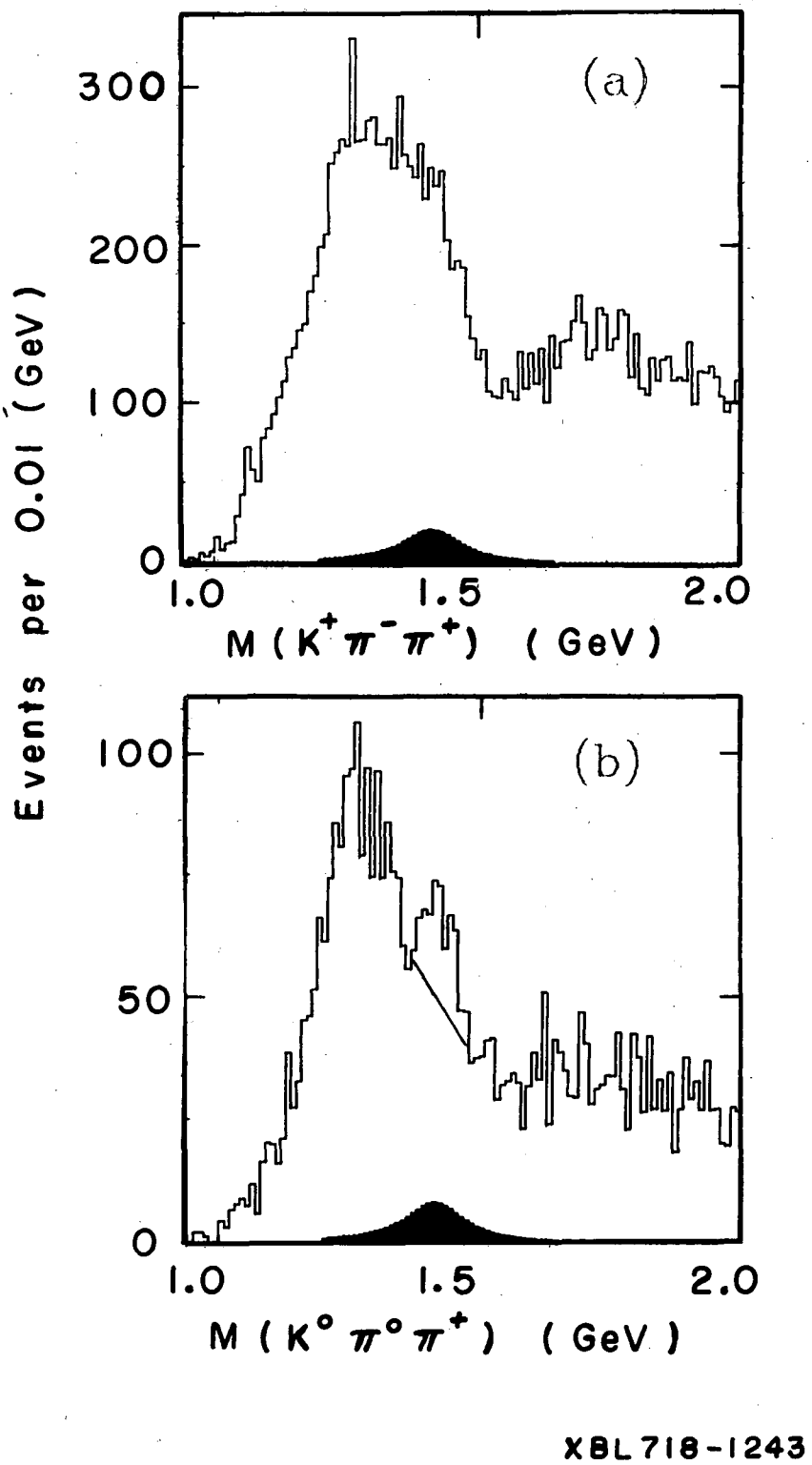
(a)
300
200
100
0
1.0
1.5
2.0
M (K⁺ π⁻ π⁺) (GeV)
Events per 0.01 (GeV)
(b)
100
50
0
1.0
1.5
2.0
M (K° π° π⁺) (GeV)
XBL718-1243

Fig. 1

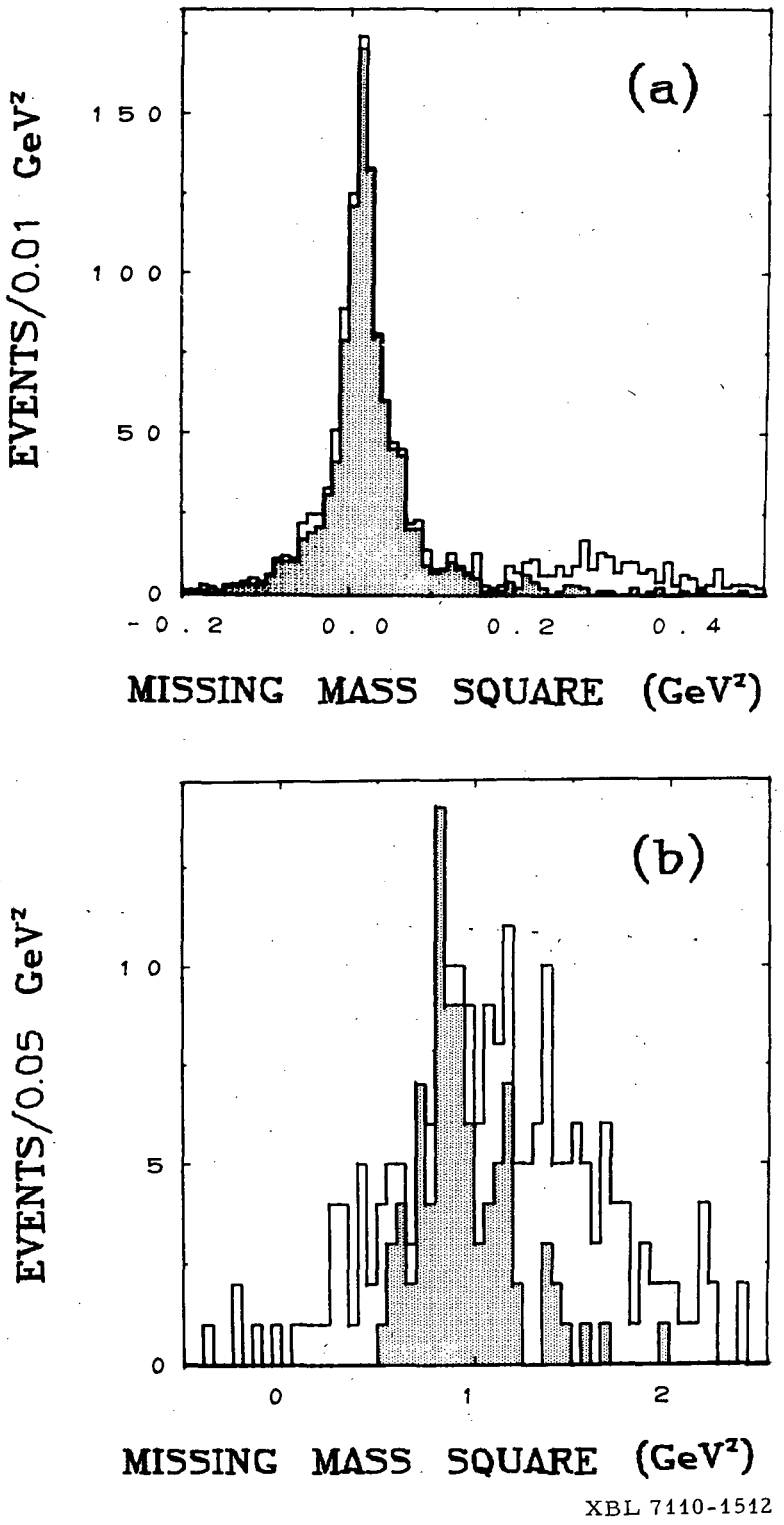
(a)
EVENTS/0.01 GeV²
150
100
50
0
-0.2
0.0
0.2
0.4
MISSING MASS SQUARE (GeV²)
(b)
EVENTS/0.05 GeV²
10
5
0
0
1
2
MISSING MASS SQUARE (GeV²)
XBL 7110-1512

Fig. 2

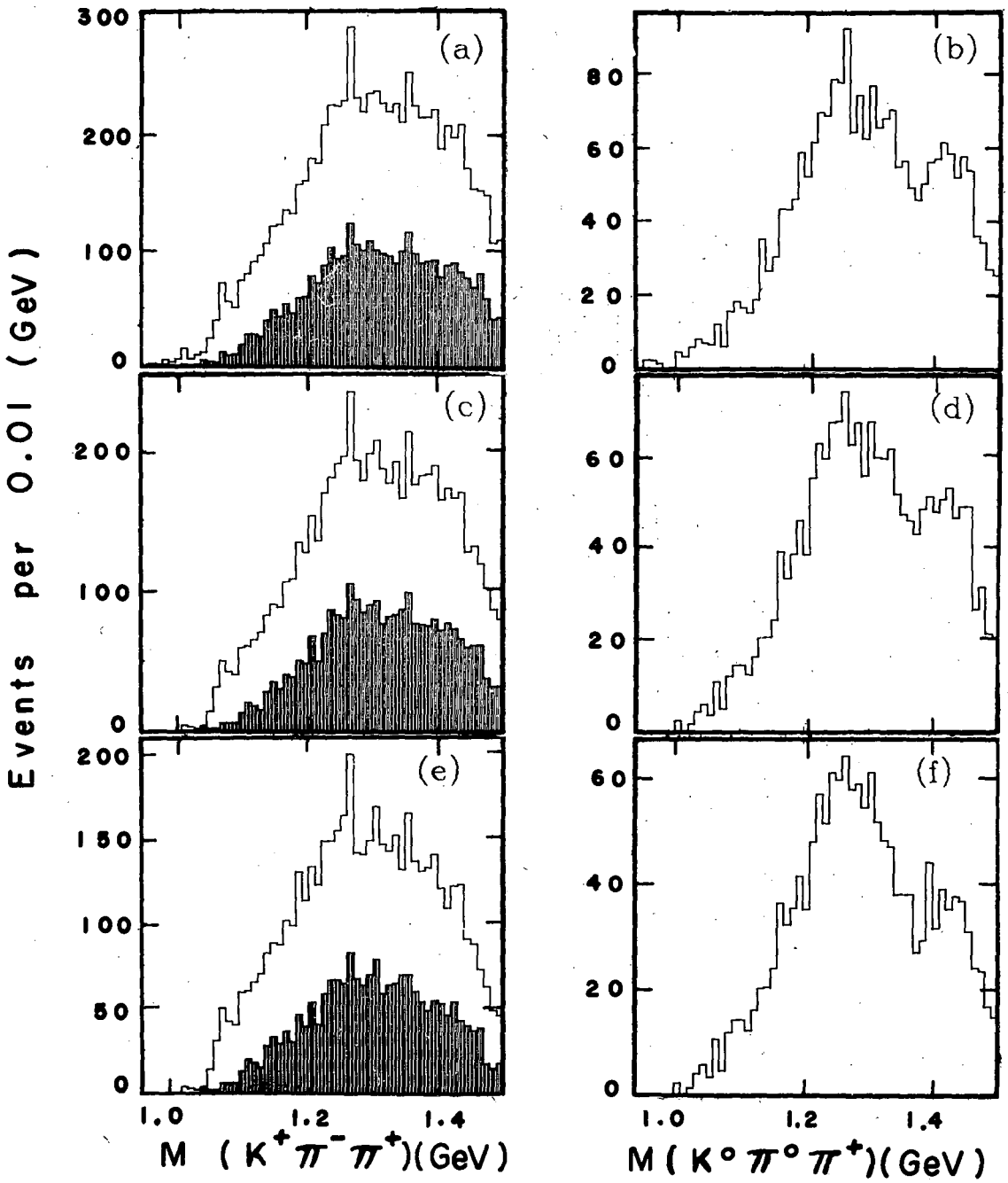
Events per 0.01 (GeV)
(a)
(b)
(c)
(d)
(e)
(f)
M (K⁺π⁻π⁺)(GeV)
M (K°π°π⁺)(GeV)
1.0
1.2
1.4
XBL718-1246

Fig. 3

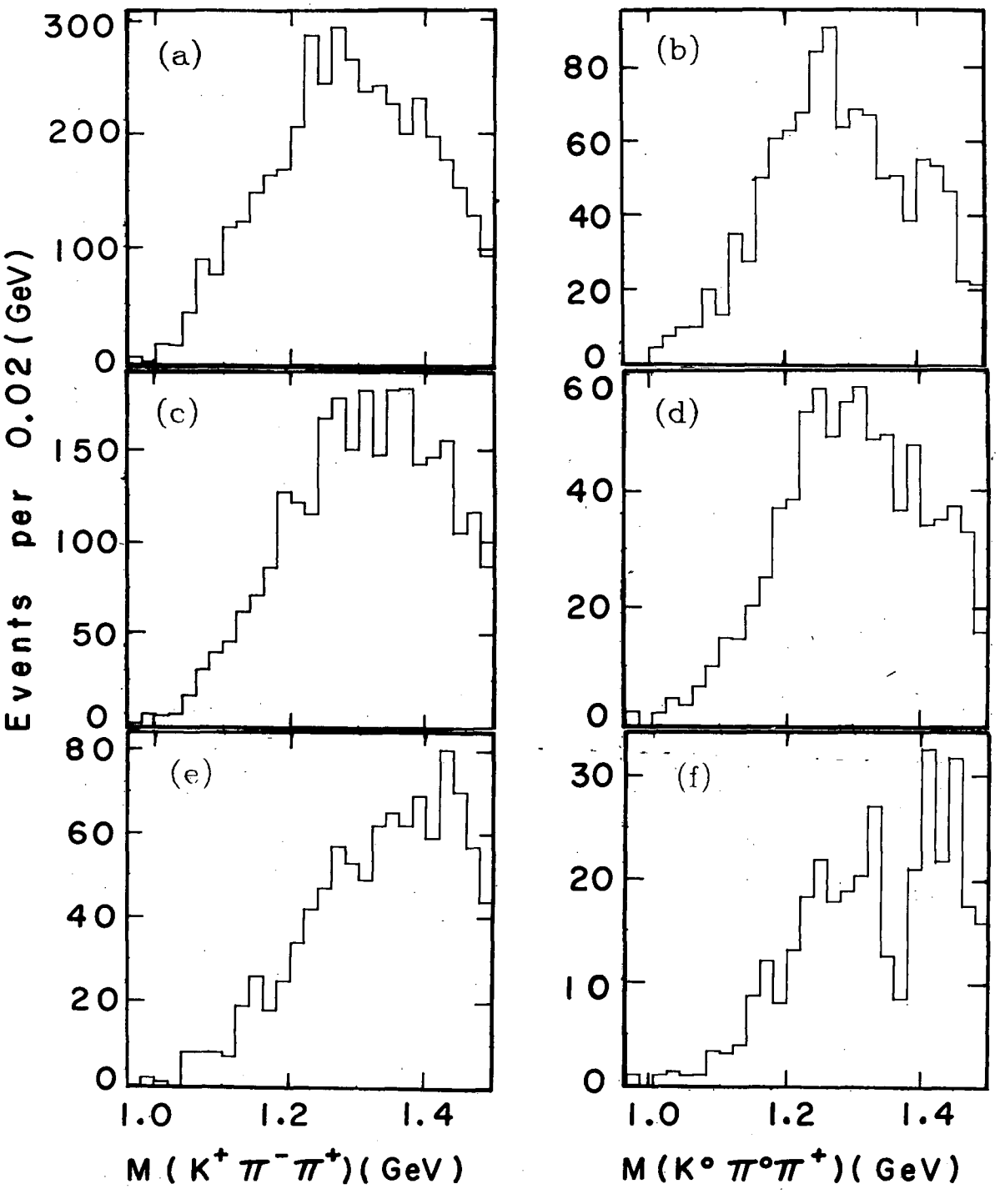

Fig. 4

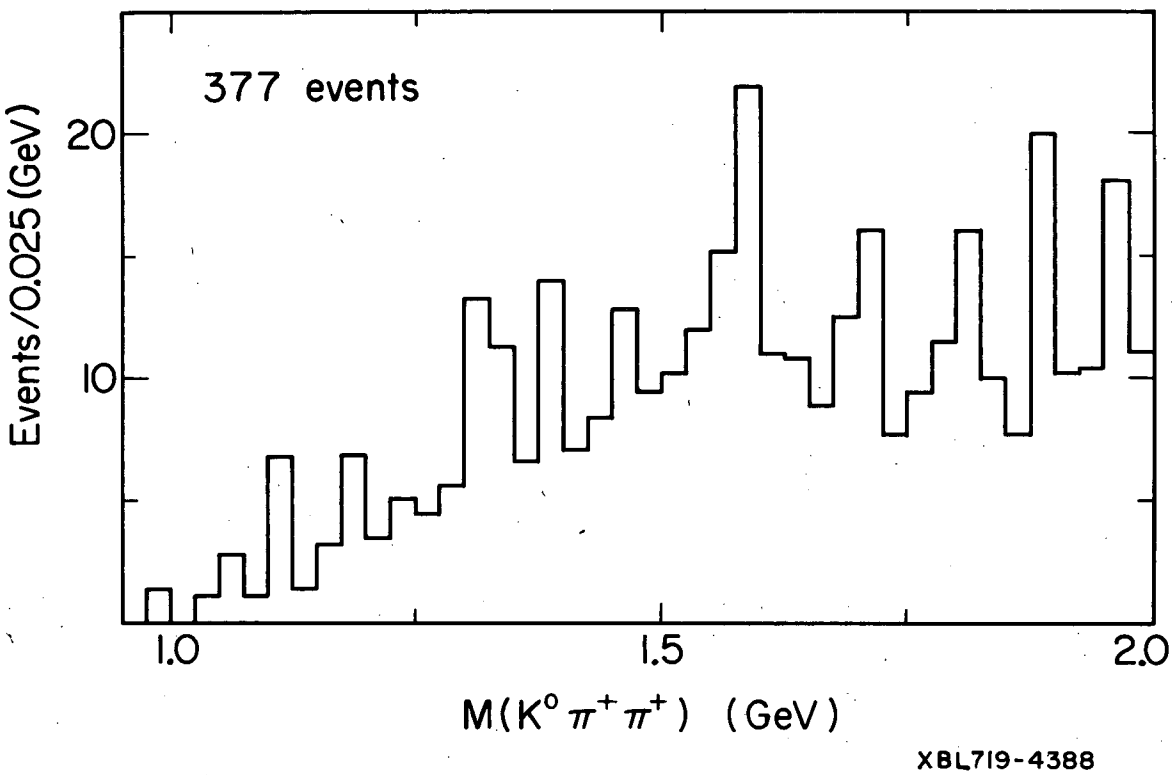

Fig. 5

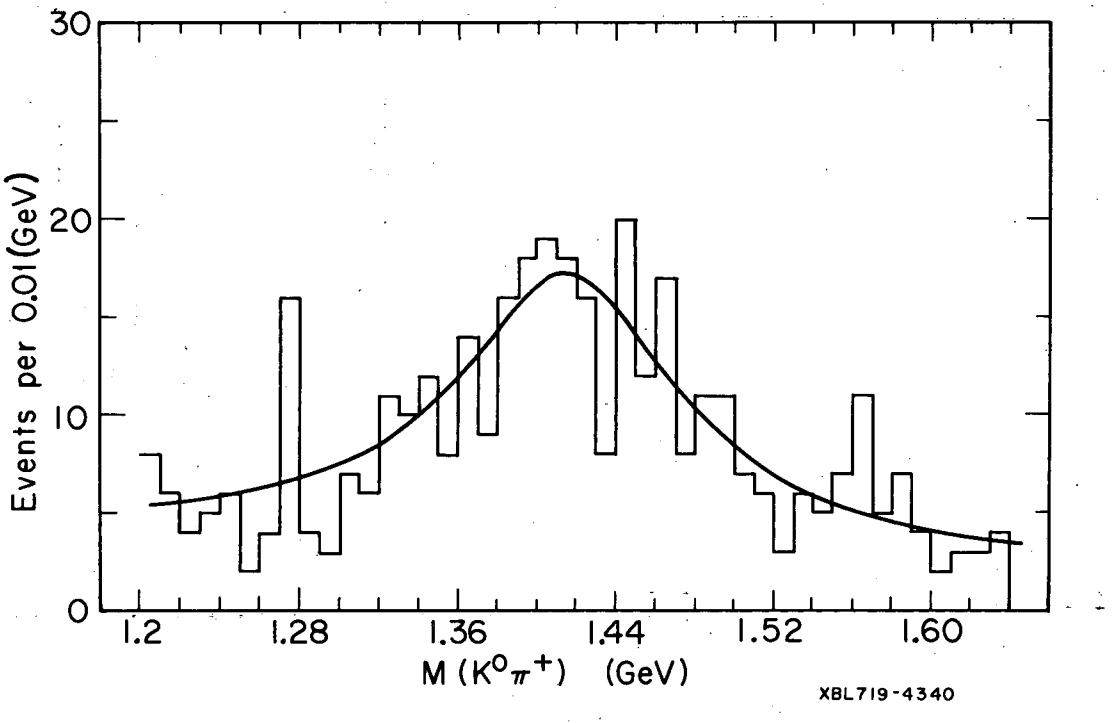
30
20
10
0
Events per 0.01(GeV)
1.2
1.28
1.36
1.44
1.52
1.60
M (K⁰π⁺) (GeV)
XBL719-4340

Fig. 6

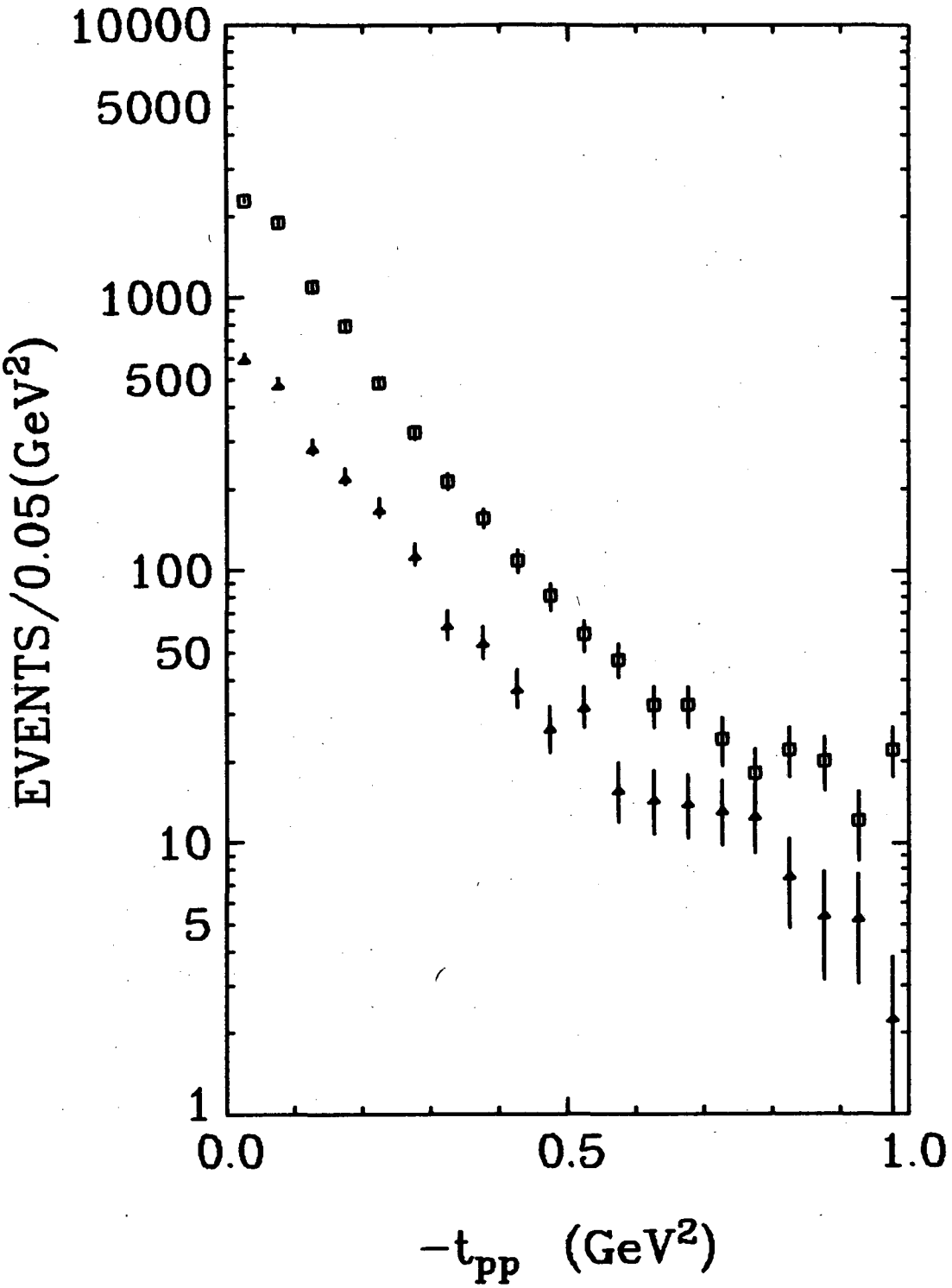

XBL 719-1401

Fig. 7

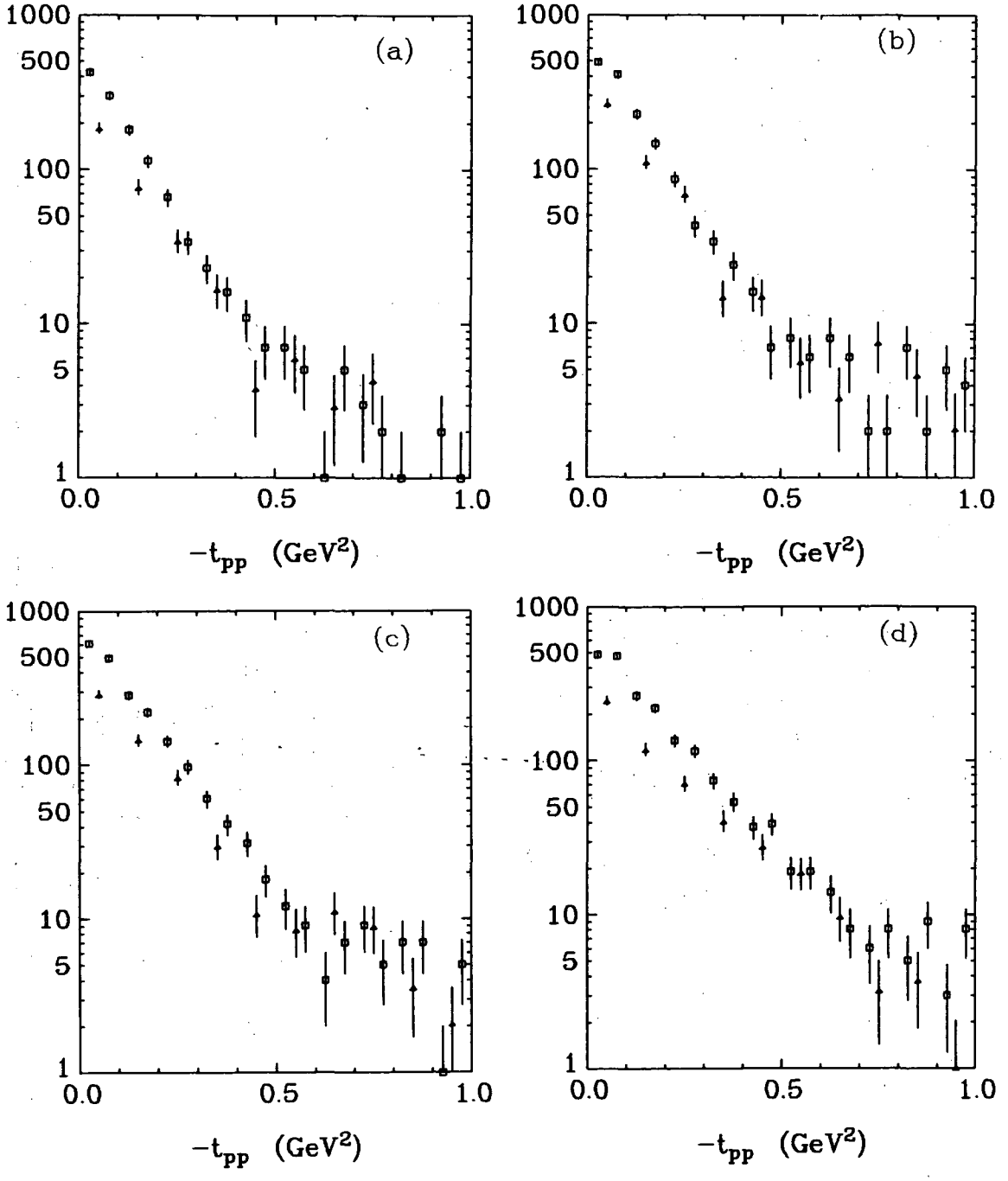

Fig. 8

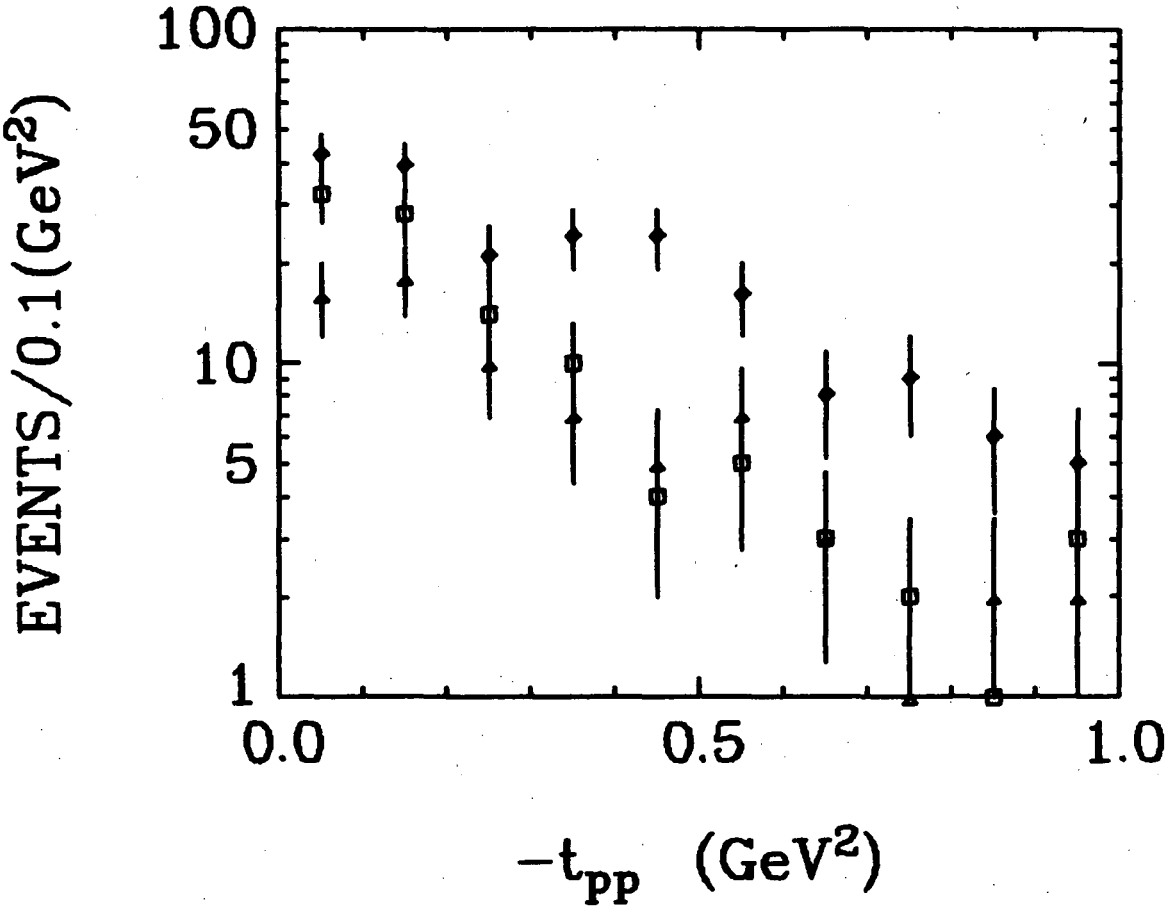

XBL 719-1402

Fig. 9

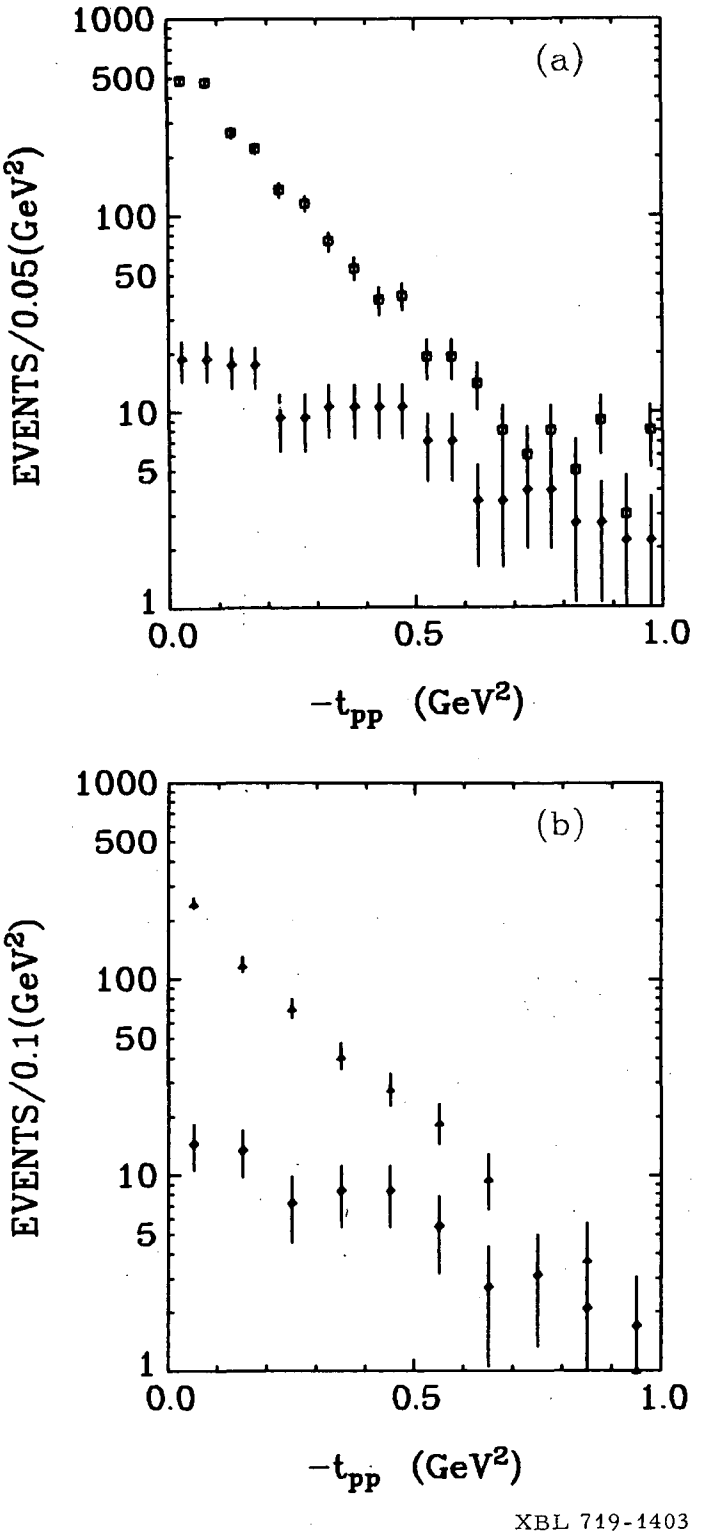
(a)
EVENTS/0.05(GeV²)
1000
500
100
50
10
5
1
0.0
0.5
1.0
$-t_{pp}$ (GeV²)
(b)
EVENTS/0.1(GeV²)
1000
500
100
50
10
5
1
0.0
0.5
1.0
$-t_{pp}$ (GeV²)
XBL 719-1403

Fig. 10

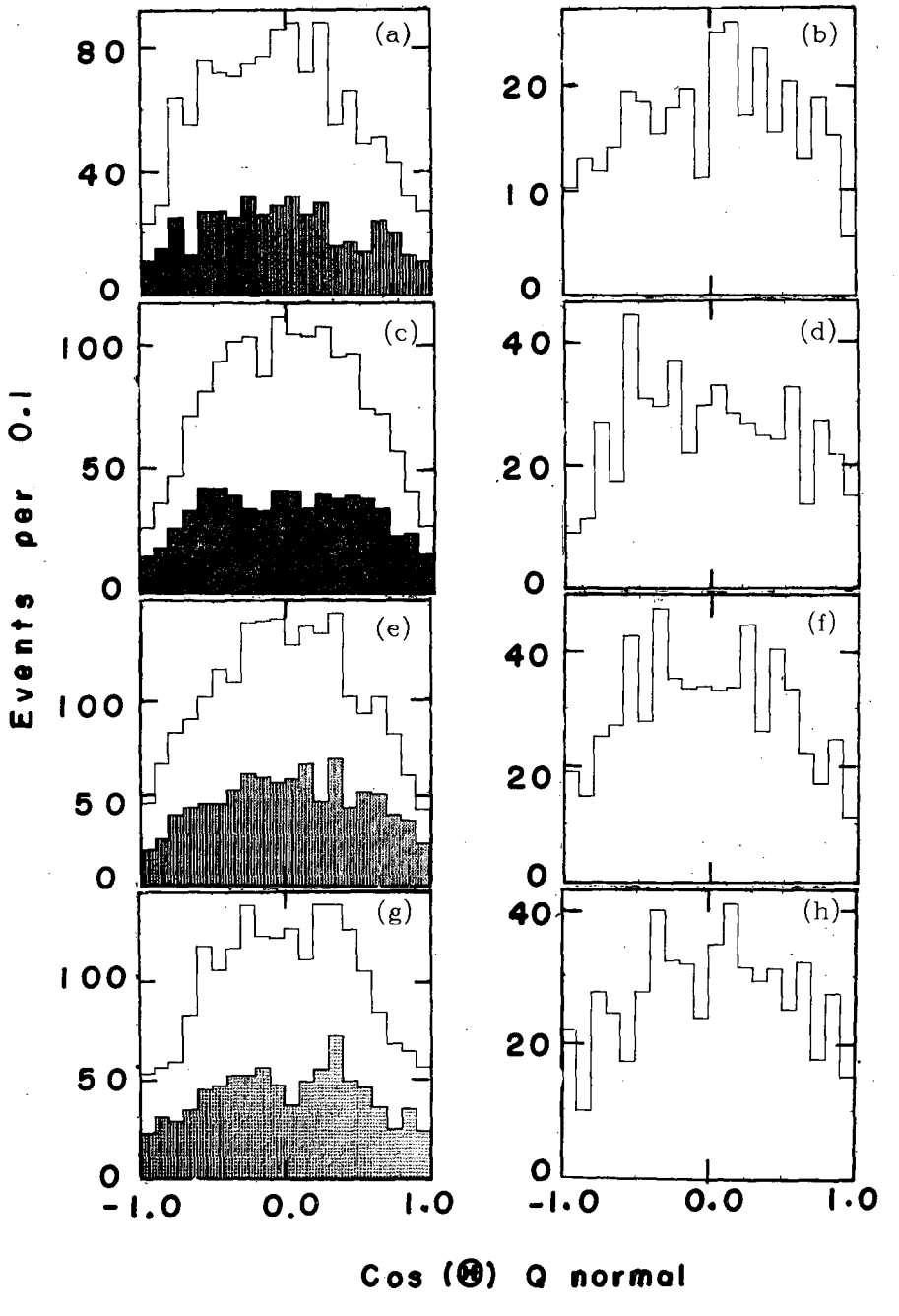

Fig. 11

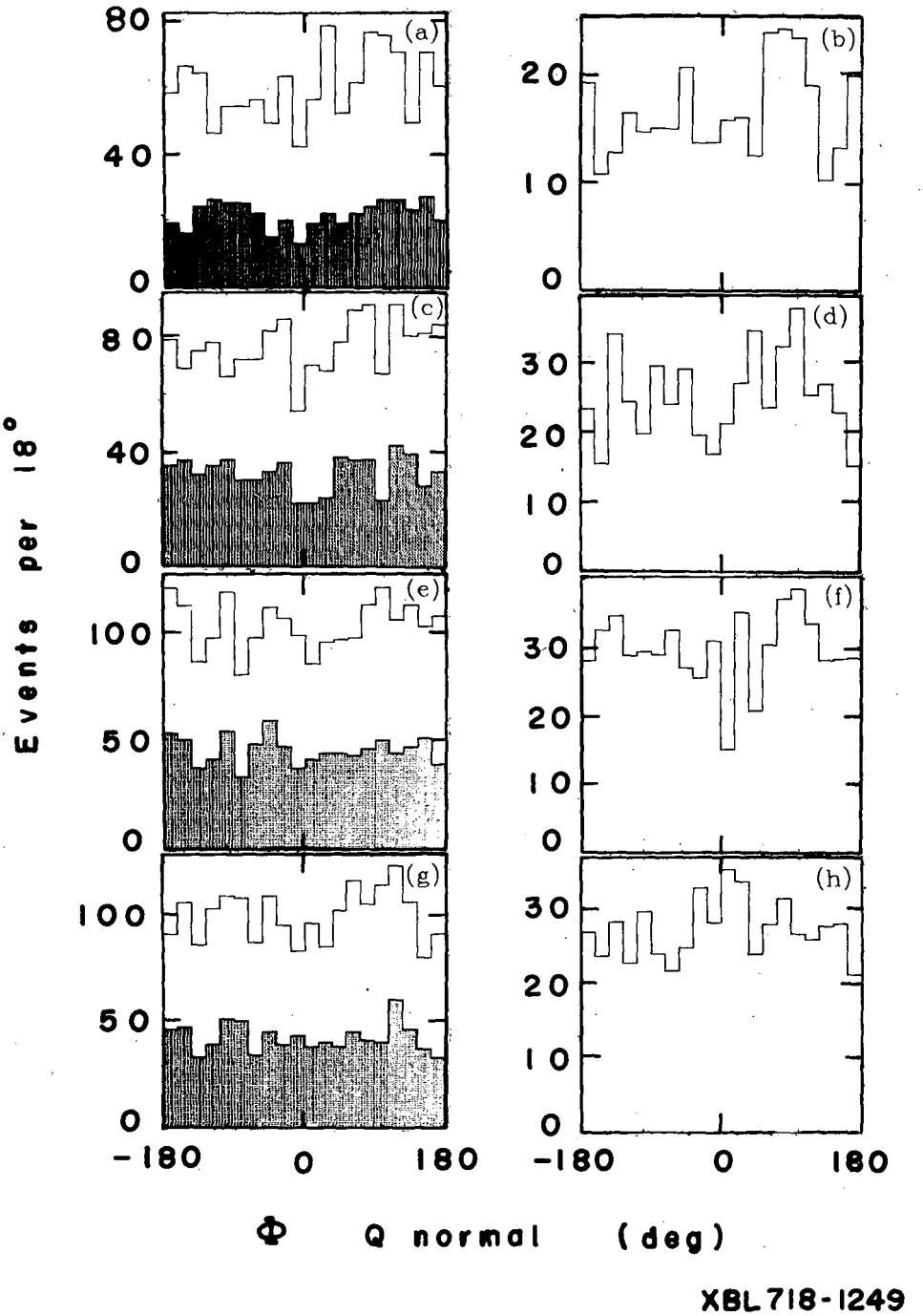

Fig. 12

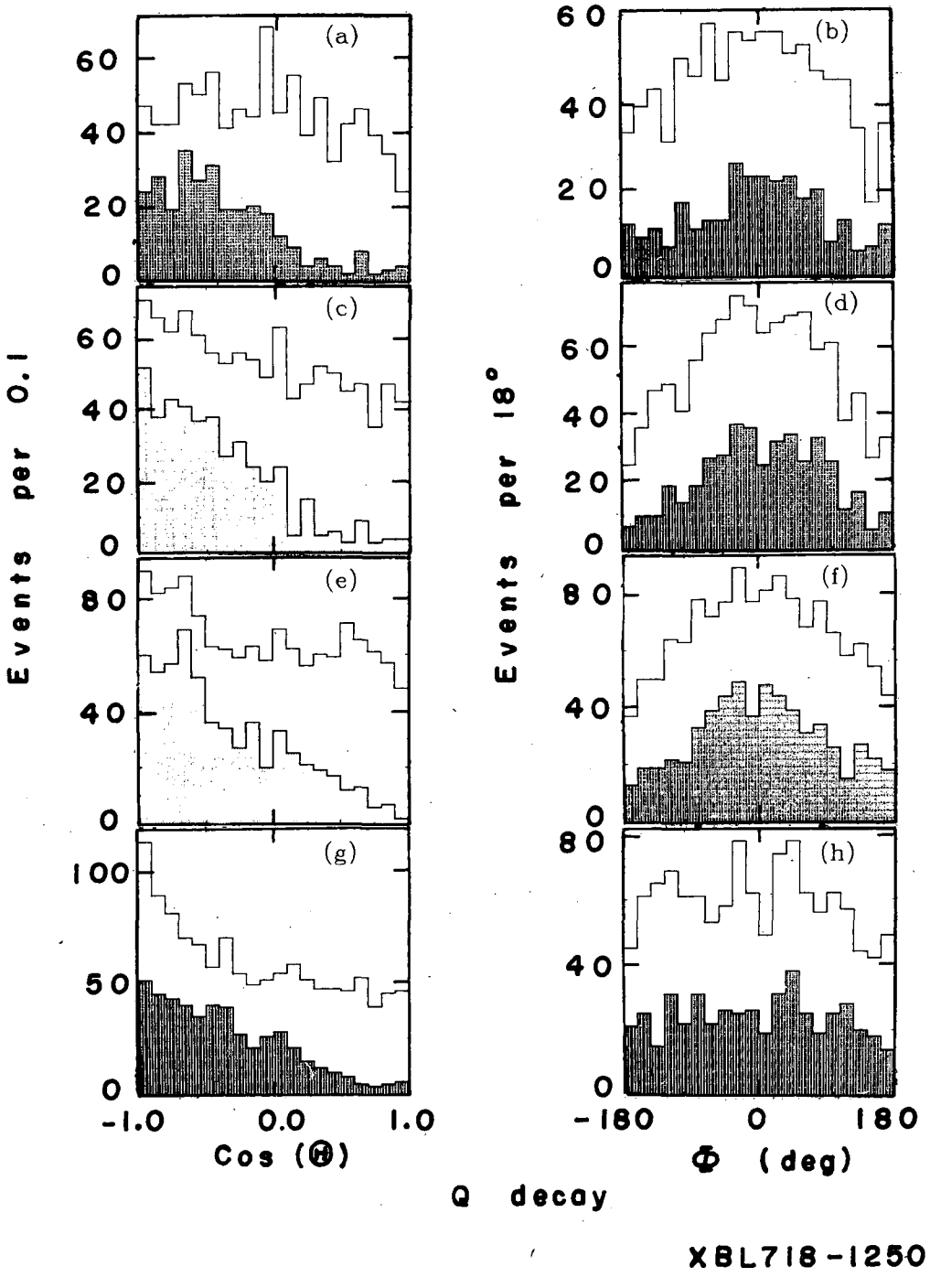
(a)
(b)
(c)
(d)
(e)
(f)
(g)
(h)
Events per 0.1
Events per 18°
Cos (Θ)
Φ (deg)
-1.0
0.0
1.0
-180
0
180
Q decay
XBL718-1250

Fig. 13

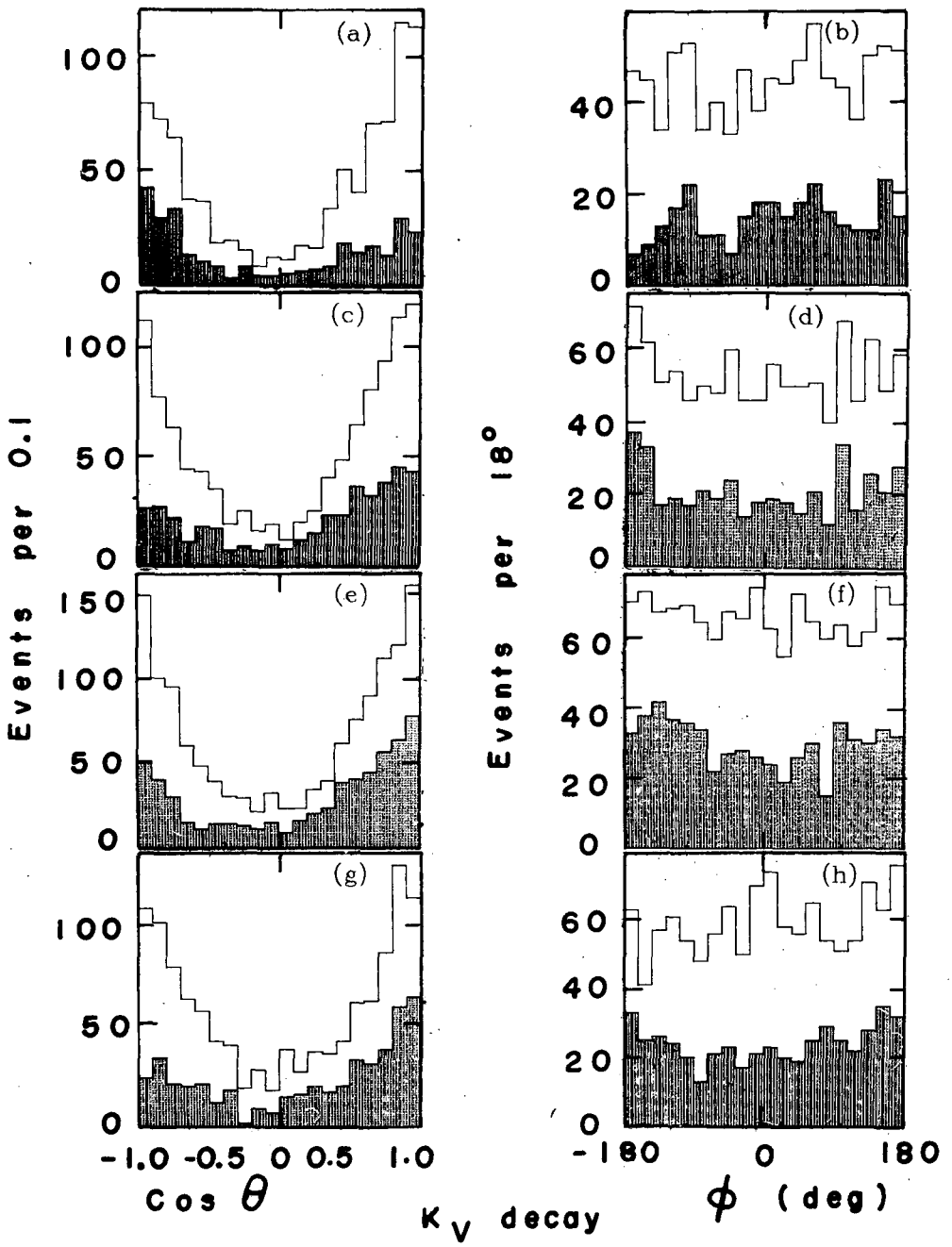
(a)
(b)
(c)
(d)
(e)
(f)
(g)
(h)
Events per 0.1
Events per 18°
Cos θ
φ (deg)
K_V decay
XBL 718 -1251

Fig. 14

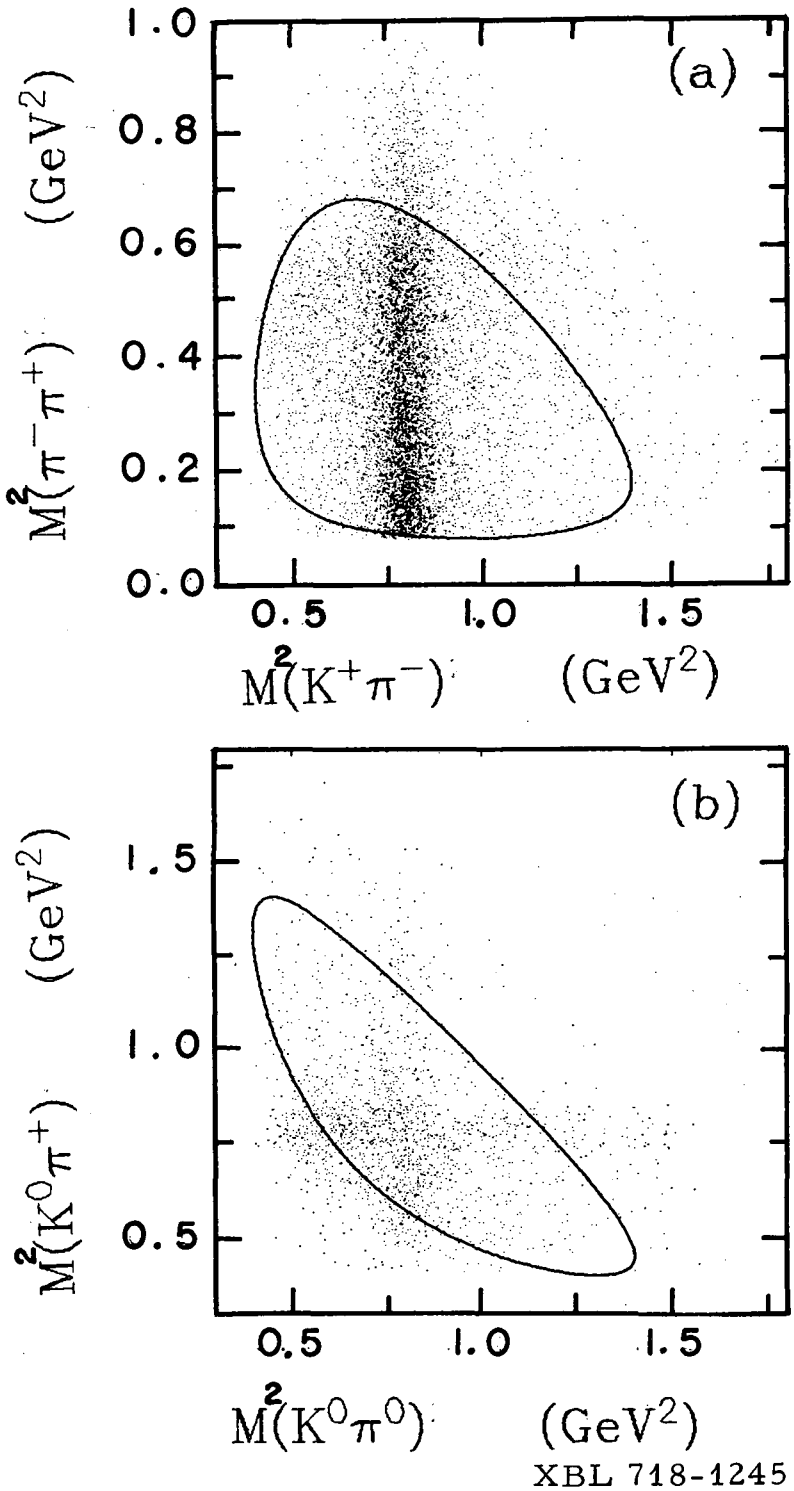
(a)
1.0
0.8
0.6
0.4
0.2
0.0
0.5
1.0
1.5
$M^2(\pi^-\pi^+)$ (GeV^2)
$M^2(K^+\pi^-)$ (GeV^2)
(b)
1.5
1.0
0.5
0.5
1.0
1.5
$M^2(K^0\pi^+)$ (GeV^2)
$M^2(K^0\pi^0)$ (GeV^2)
XBL 718-1245

Fig. 15

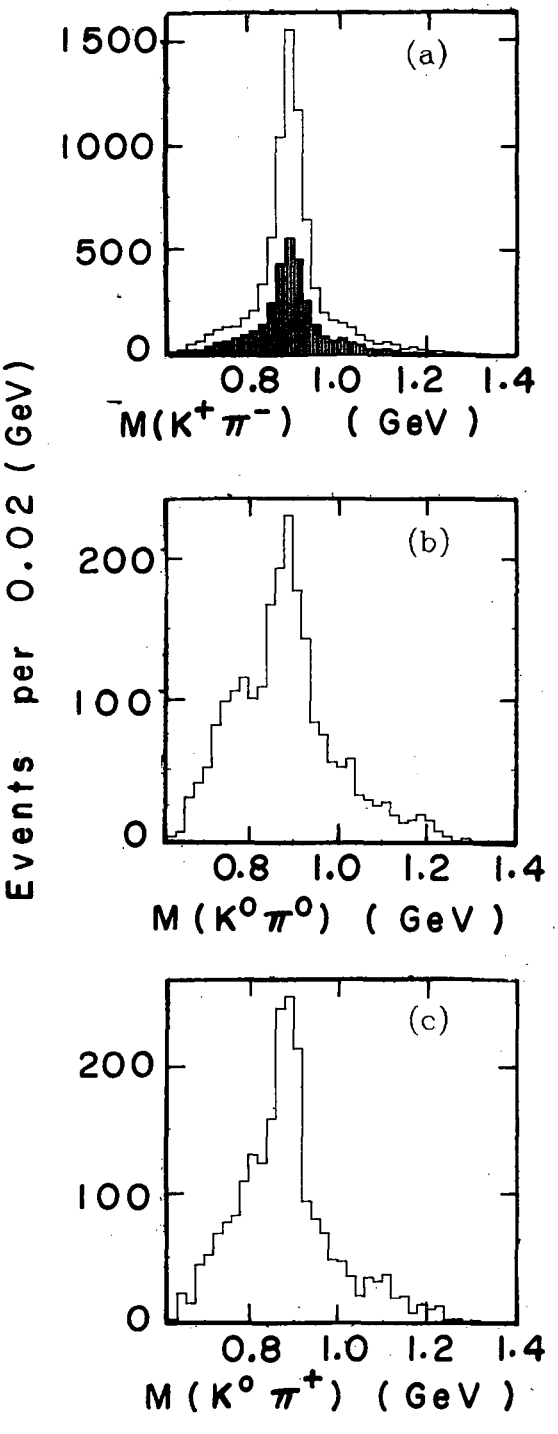
(a)
1500
1000
500
0
0.8 1.0 1.2 1.4
M(K⁺π⁻) (GeV)
(b)
200
100
0
0.8 1.0 1.2 1.4
M(K⁰π⁰) (GeV)
(c)
200
100
0
0.8 1.0 1.2 1.4
M(K⁰π⁺) (GeV)
Events per 0.02 (GeV)
XBL718-1247

Fig. 16

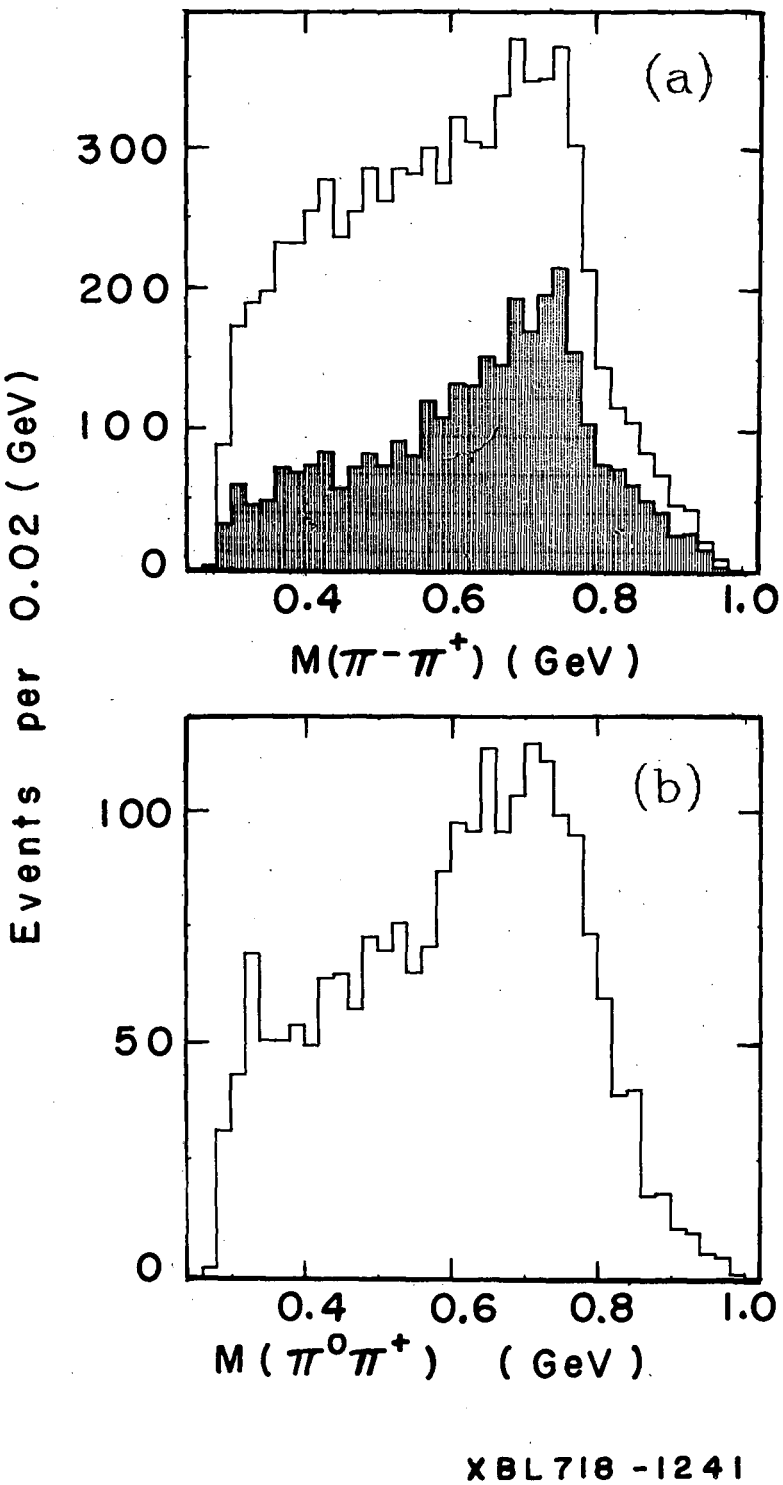
(a)
300
200
100
0
0.4
0.6
0.8
1.0
M(π⁻π⁺) (GeV)
Events per 0.02 (GeV)
(b)
100
50
0
0.4
0.6
0.8
1.0
M (π⁰π⁺) (GeV)
XBL718 -1241

Fig. 17

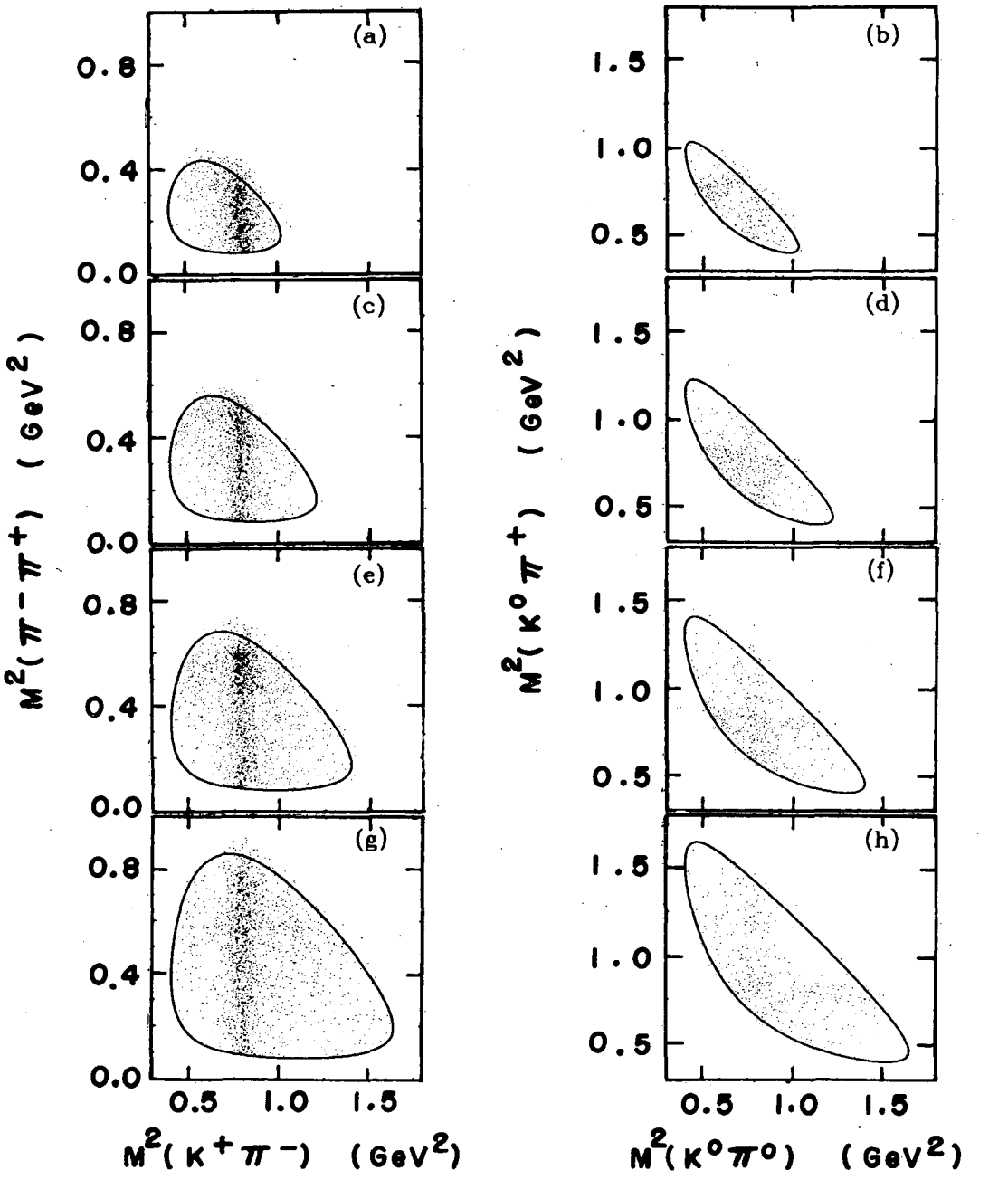
(a)
(b)
(c)
(d)
(e)
(f)
(g)
(h)
0.8
0.4
0.0
1.5
1.0
0.5
$M^2(\pi^-\pi^+)$ (GeV^2)
$M^2(K^0\pi^+)$ (GeV^2)
0.5 1.0 1.5
$M^2(K^+\pi^-)$ (GeV^2)
$M^2(K^0\pi^0)$ (GeV^2)
XBL718 - 1252

Fig. 18

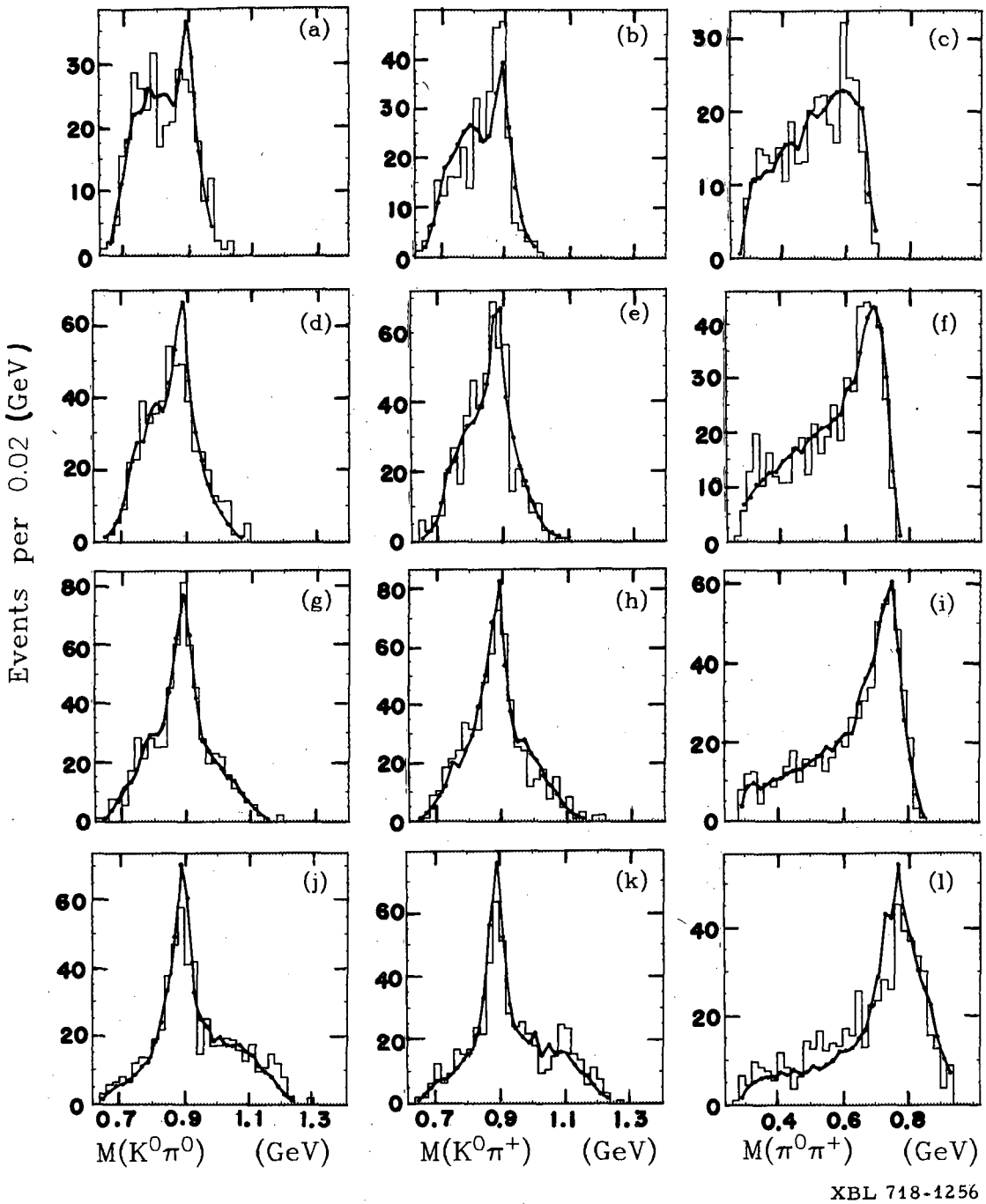
(a)
(b)
(c)
(d)
(e)
(f)
(g)
(h)
(i)
(j)
(k)
(l)
Events per 0.02 (GeV)
0.7 0.9 1.1 1.3
M(K⁰π⁰) (GeV)
0.7 0.9 1.1 1.3
M(K⁰π⁺) (GeV)
0.4 0.6 0.8
M(π⁰π⁺) (GeV)
XBL 718-1256

Fig. 19

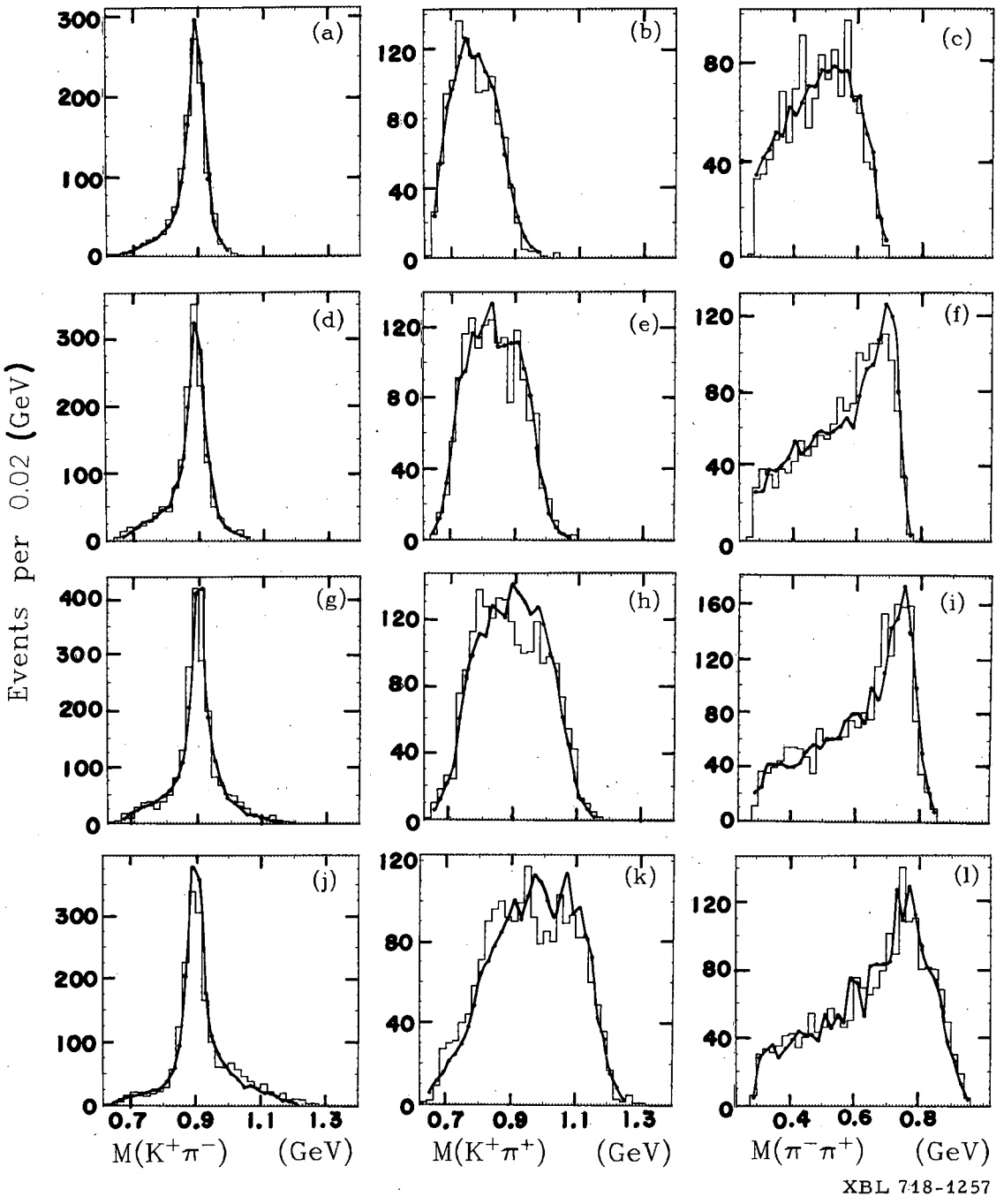
(a)
(b)
(c)
(d)
(e)
(f)
(g)
(h)
(i)
(j)
(k)
(l)
Events per 0.02 (GeV)
M(K⁺π⁻) (GeV)
M(K⁺π⁺) (GeV)
M(π⁻π⁺) (GeV)
XBL 718-1257

Fig. 20

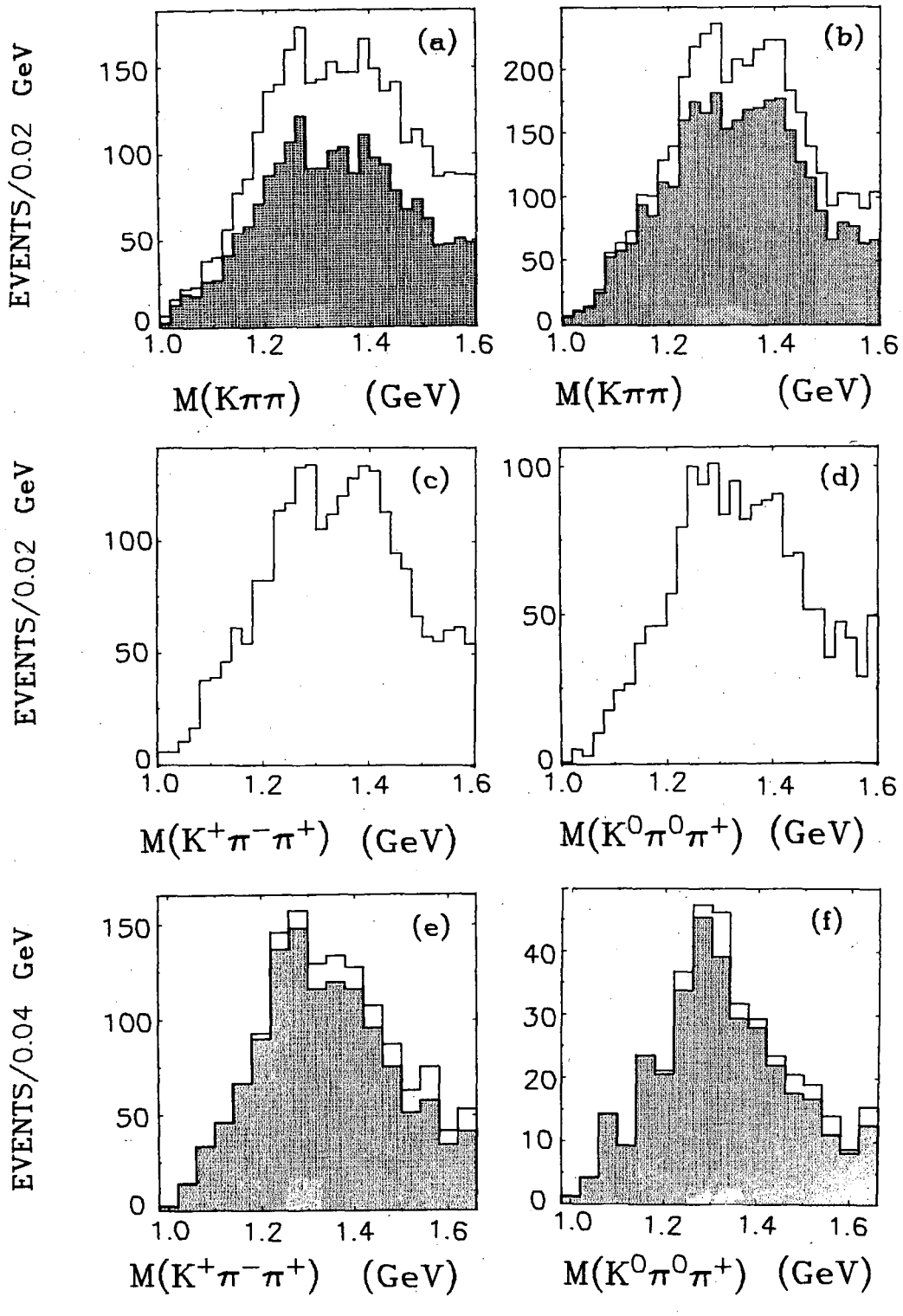

XBL 7110-1513

Fig. 21

TECHNICAL INFORMATION DIVISION
LAWRENCE BERKELEY LABORATORY
UNIVERSITY OF CALIFORNIA
BERKELEY, CALIFORNIA 94720